Bulletin of the New Zealand Society for Earthquake Engineering, Vol. 57, No. 4, December 2024

EARTHQUAKE DESIGN PRESSURES FROM SOIL INTERACTION ON BUILDING BASEMENT WALLS

John H. Wood[1]

(Submitted *July 2024*; Reviewed *August 2024*; Accepted *September 2024*)

ABSTRACT

Free-standing retaining walls supporting a cohesionless soil backfill are usually designed for earthquake induced soil pressures using the Mononobe-Okabe limit state analysis (Mononobe and Matsuo [1]). This method assumes the development of a failure wedge in the backfill soil leading to active soil pressures on the wall. Building basement walls are usually relatively stiff or restrained from relative displacement so the active pressure state is unlikely to arise. In addition, two components of dynamic pressure that develop on the wall need to be considered. The first of these is due the shear deformations in the soil generated by the earthquake waves. The second results from the inertia forces of the building above ground level generating movements of the wall against the soil.

Two-dimensional elastic finite element analyses were undertaken in the present study to determine the earthquake induced pressure force and its distribution on simplified basement wall structures. The parameters investigated included the width and stiffness of the basement, the depth of the soil layer and the distribution of the soil shear modulus with depth.

Because of the wide range of basement geometries and foundation types it is not possible to develop a simple empirical method that is widely applicable. However, the elastic finite element analyses identified the influence of the most important parameters and the results can be used to decide whether more detailed analyses are necessary for large buildings.

https://doi.org/10.5459/bnzsee.1704

INTRODUCTION

The evaluation of seismic earth pressures should consider soil structure interaction involving the wall, the supporting and retained soil and any attached structure. Both kinematic and inertial components can be significant. Kinematic seismic pressures are produced by the combined seismic excitation of the site soil and the wall system embedded in the soil by propagating earthquake waves. Inertial seismic earth pressures are significant when the basement wall structure is supporting a multi-storey building. The base shear and overturning moment generated by the inertia forces from the building cause the basement to displace horizontally and rotate producing soil pressures against the external walls.

There are not many published documents describing damage to engineered retaining structures or basement walls in recent earthquakes. A possible reason is that earthquake damage to walls is often relatively minor in comparison to damage sustained by multi-storey buildings and major civil engineering structures. For basement walls, a further reason is that they are usually designed for at-rest gravity soil pressures and for serviceability against ground water ingress. This results in robust walls with good resistance to earthquake induced soil pressures.

Quite extensive damage to free standing wall structures occurred in the 2010-11 Canterbury earthquake sequence and is reported in a number of published papers including: Anderson et al [2], Dismuke [3], Riches [4], Stone et al [5] and Wood [6]. Most of the damaged walls were located on relatively steep terrain in the Port Hills region of Christchurch and were of a variety of construction types including timber poles, gabion, crib, concrete and stone masonry. Damage to these walls is not very relevant to assessing basement wall performance; however, Wood [6] reported damage to concrete masonry walls in the basement of a residential building. Apparently, there was damage to a number of residential basement walls but there are no published reports describing this damage.

A revision of the New Zealand National Seismic Hazard Model (NSHM) led by GNS Science was completed in 2022 (Gerstenberger et al [7]). In many parts of New Zealand this new model shows a significant increase in hazard from the 2000 model (Stirling et al [8]) which formed the basis of the current Earthquake Loading Design Code (NZS1170.5 [9]). This increase is illustrated in Figure 1 which shows for the main city centres a comparison of the Peak Ground Acceleration (PGA) for a 500-year return period (Annual Probability of Exceedance, APE of 1/500) given in the current earthquake loadings code with the Draft Earthquake Loading Code (DZ TS 1170.5 [10]) which is based on the 2022 NSHM. In some centres, particularly those in the lower part of the North Island, the proposed PGA's have increased by more than 50%.

Since the kinematic wall pressures from interaction with the earthquake waves are directly related to the PGA this change will result in earthquake induced pressures becoming a much more important consideration in basement wall design than previously. On some buildings, after making allowance for load combination load factors, the combination of earthquake and gravity load pressures will dominant over those from gravity alone.

Extensive research involving both analytical and experimental studies has been carried out on earthquake induced soil pressures on free-standing retaining walls and design analysis procedures are well established (for example the Mononobe-

[1] *Retired Civil Engineer, Lower Hutt, john.wood@xtra.co (Life Member).*

Okabe method). In contrast studies on the earthquake induced soil pressures on building basement walls is limited. While recent research has acknowledged that embedded basement walls should be considered in the building seismic design, no specific provisions that consider both the kinematic and inertial components have been adopted.

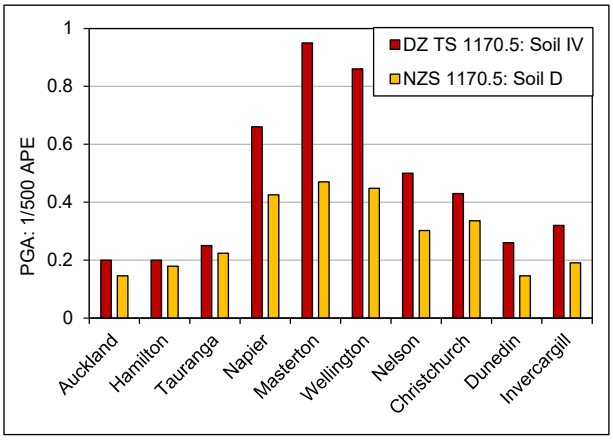

Figure 1: Comparison of design code PGA's for 1/500 APE.

Two-dimensional elastic finite element analyses (FEA) were undertaken as part of the present study to determine the earthquake induced pressure force and its distribution on basement walls. For the kinematic component, the parameters investigated included the width and stiffness of the basement, the depth of the soil layer and the distribution of the soil modulus with depth. The analyses were verified using results from a recent research project involving wall pressure measurements on a centrifuge model. For the building inertia force component, the basement was assumed to be rigid but to displace by both horizontal translation and rotation about the horizontal centreline. For this component, the influence of the soil layer depth and modulus distribution on the wall pressures were also investigated.

A number of recent experimental and analytical studies investigate the wall pressures arising from the kinematic wave generated soil deformations. Most of the analytical studies consider buildings founded on rock or very stiff soil but these are not typical foundations of many buildings that have basements founded on piles or on a raft foundation. Several of the frequently referenced studies on earthquake induced soil pressures on basement walls are summarised in the following sections.

Ostadan Method

The method proposed by Ostadan [11] to estimate earthquake pressures involves carrying out a one-dimensional soil column analysis (using a computer program such as SHAKE, Schnabel et al [12]) to obtain the response in terms of a 30% damped acceleration response spectrum at the depth corresponding to the base of the wall in the free-field. An empirical equation was then used to compute the equivalent mass of the soil layer interacting with the wall which is assumed to represent a single degree of freedom system. The lateral seismic force on the wall was computed from the product of the equivalent mass and the spectral acceleration at the frequency of the soil column at the base of the wall. The maximum lateral seismic soil pressure at the ground surface level was obtained by dividing the lateral force obtained by the area under a normalized seismic soil pressure distribution. The pressure profile was obtained from the peak pressure and an empirical pressure distribution relationship.

Ostadan compared the seismic soil pressure results obtained for a 9.2 m high building basement wall embedded in a soil layer with shear wave velocity of 305 m/s using the Mononobe-Okabe (M-O), the rigid wall method of Wood [13] and his simplified method. Results are shown in Figure 2. For the simplified method, all the ground motions were scaled to a PGA of 0.3 g. The M-O method and the Wood solution require only the PGA as input. For the M-O method, it was assumed that the seismic soil pressure has an inverted triangular distribution (maximum at the top). As shown in Figure 2, the M-O method results in the lowest pressures and the Wood solution generally results in the maximum soil pressures. The Ostadan method results in a range of pressure profiles, depending on the frequency content of the input motion.

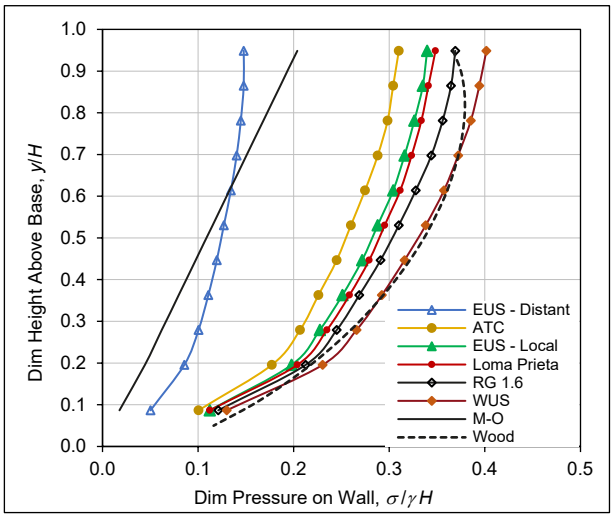

Figure 2: Comparison of earthquake soil pressures. From Ostadan [11] (modified).

British Columbia

Taiebat et al [14] report a major study on the behaviour of basement walls during earthquakes. For the study a typical four-storey basement wall structure was designed for different fractions of the design level PGA for Vancouver, British Columbia. The current practice for the seismic design of basement walls in British Columbia is to use the M–O method with an inverted triangular pressure distribution and the PGA of the design ground motion. The 2010 National Building Code of Canada [15] specifies for building design a seismic hazard level of 2% in 50 years, which gives a PGA of 0.46*g* in Vancouver.

Dynamic nonlinear soil–structure interaction analyses were conducted on numerical models of the walls. The flexibility and yield moments of the wall structure were taken into account and the soil layers modelled using a Mohr–Coulomb failure criterion. A degraded elastic modulus and equivalent damping ratio were employed to give a close representation of the soil response under seismic loading. The soil–basement wall system was subjected to a suite of seven ground motions matched to the design ultimate hazard spectrum for Vancouver. Results of the numerical study were presented in the form of time histories of lateral soil force on the walls and its height of application above the wall base, envelopes of maximum and minimum lateral earth pressure, profiles of earth pressures at maximum lateral force. Envelopes of bending moments, shear forces, lateral deformations, and drift ratios over the height of the walls were also presented. The drift ratios were a measure of yield deformation from plastic hinge rotations in the walls. A 2% drift ratio, based on the ASCE Guidelines for *Design of Blast-resistant Buildings in Petrochemical Facilities* [16] was considered acceptable.

The top basement level was found to be the most critical. The height of the wall in this level was 3.6 m and greater than the 2.7 m height of the walls in the lower basement levels. Also, the

wall was not restrained at the top as was the case for the lower basement levels. The sensitivity of the results to variations in the soil constitutive model was evaluated. It was concluded that basement walls founded on dense soil can be safely designed using the M–O method, but with an acceleration of 50%–60% PGA instead of 100% PGA.

Amirzehni et al [17] report on extensions of the Taiebat et al, study to deeper basement walls founded on a different soil profile. Also, a more representative nonlinear hysteretic model was used to characterize the hysteretic stress-strain response of soil. The results provided further evidence of acceptable seismic performance of basement walls designed using the M-O method with an acceleration significantly less than the code level PGA.

Centrifuge Tests

A number of centrifuge tests have been carried out by researchers at the University of California on 1/36 scale model walls that represent both basement and stiff wall structures. The scale of the models allowed the structures to be founded on soil instead of being mounted directly on a rigid base as has been the case in most shaking table tests. Experiments reported by Mikola and Sitar [18] and Candia and Sitar [19] modelled fixed-base free-standing cantilever structures retaining cohesionless and cohesive soils. All of the walls were 6.5 m high in prototype scale and were founded on a 13.5 m deep soil layer. An experiment by Wagner and Sitar [20] modelled a 13.3 m deep braced basement type wall structure retaining cohesionless soil and founded on a 6.7 m deep soil layer. The geometry of the structure and the extent of the soil backfill and founding soil layer is shown schematically in Figure 3. The soil layer and backfill are drawn approximately to scale.

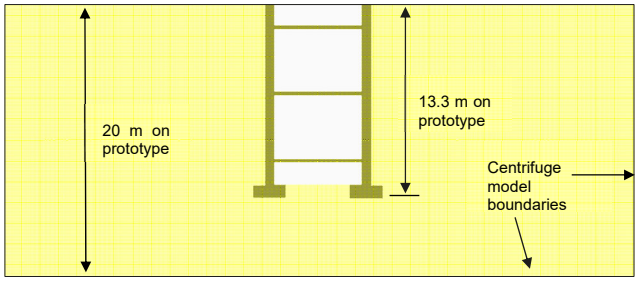

Figure 3: 13.3 m deep model basement wall structure studied by Wagner and Sitar [20].

Wagner and Sitar also carried out numerical studies using the FLAC software [21] to simulate the centrifuge study of the 13.3 m deep basement model. Numerical work was extended to include basements with three 8 m wide bays and overall depths of 3, 6, 9 and 12 m.

The dynamic earth pressures in the centrifuge experiment were estimated by removing the wall inertia loads (using recorded accelerations) from forces measured by load cells installed in the bracing beams between the wall members and distributing the adjusted forces using tributary areas. The soil pressures on the walls in the numerical simulation were interpreted from both the axial loads in the bracing beams and the dynamic earth pressures in the soil mesh adjacent to the wall members. Typical experimental and numerical dynamic earth pressure distributions corresponding to the maximum dynamic force pressure increment are shown in Figure 4 for the Kobe Tatatori 090 input acceleration time-history input motion which produces an average free-field PGA of 0.5 g on the model. The experimental and numerical results are compared with the M-O and the Seed and Whitman [22] (S-W) pressure distributions. The S-W method is based on M-O but with the centre of pressure at 0.6 of the wall height from the base. The M-O distribution was computed using the maximum averaged acceleration over the depth of embedment of the basement. The S-W, dynamic earth pressure distribution was computed using 80% of the PGA at the ground surface.

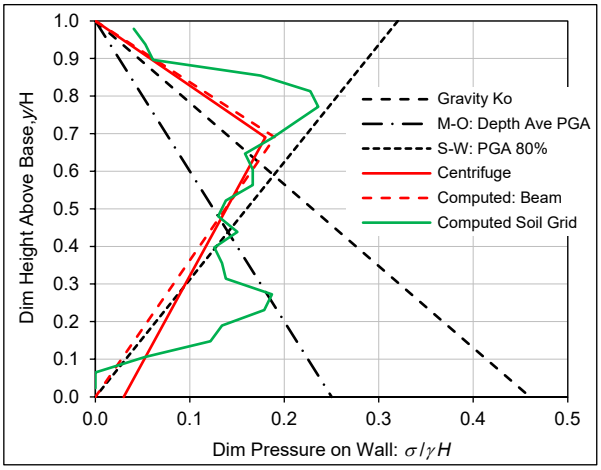

Figure 4: Pressure comparisons – computed and centrifuge for acceleration time-history. From Wagner and Sitar [20].

The Wagner and Sitar 13.3 m deep basement structure was analysed in the present study using an elastic FEA model. This indicated that because of rotations of the wall footings the basement structure was more flexible than many basement structures that are usually stiffened by end walls and intermediate dividing walls and frames. Estimating the dynamic soil pressures from the load cells in the bracing beams may have led to an underestimation of the dynamic pressures because if the soil stiffness is equal on either wall, the displacements in the first mode response of the soil layer are symmetrical about the structure centreline and for this case the theoretical axial loads in the bracing beams are zero. Higher modes of the soil layer will induce axial loads in the bracing but the first mode is likely to have the largest response. Also, the soil stiffness will vary to some extent between the wall faces as at any instance of time one will have a tension dynamic pressure component and the other a corresponding compression component. On the tension side soil gapping will develop over the top part of the wall where the gravity static pressures are low.

The elastic FEA indicated that the inertia loads from the walls increased the soil pressures so making deductions to measured bracing loads for wall inertia effects may also have introduced error.

Hushmand Reservoir Study

Hushmand et al [23] carried out a series of sixteen centrifuge model experiments on 10 to 12 m high reinforced concrete underground reservoir structures. Two-dimensional 1/60 scale models were constructed to match the mass, lateral stiffness, and natural frequency of typical prototype reservoir structures. The structural stiffness was varied by changing the thickness of the walls, roofs and base slabs and keeping the height, width, and length the same. The models were fabricated from welded steel plates to give moment connection at the corners. The stiffness of the two stiffest models was reasonably typical of basement structures of similar height.

The structures were buried in either a dry medium-dense sand or a silty sand with different slopes on the backfill surface. A suite of earthquake ground and sinusoidal motions were used with the input motion applied at the base of the soil in the centrifuge model containment bucket.

Soil pressures against the walls were measured using tactile sensors mounted on the surface of the model walls. The experimental results are of particular interest because the soil pressures were measured directly and this does not appear to have been done successfully in other reported experimental studies.

The structure stiffness, backfill soil type, surface slope, embedment depth, and input ground motion characteristics were varied to evaluate their influence on structural performance. Three of the tests were carried out using cohesionless soil with the reservoir roof at the surface of level ground (similar to a basement wall). A schematic layout of the centrifuge model and soil layer used in these tests is shown in Figure 5. The soil layer is drawn approximately to scale.

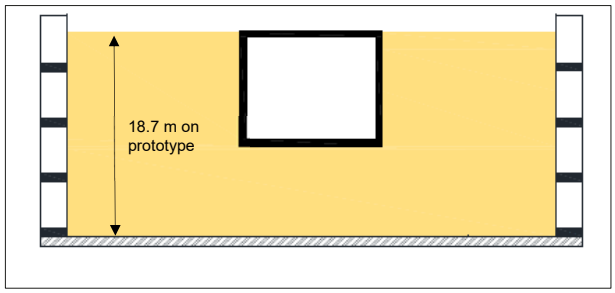

Figure 5: Centrifuge models with ground surface at roof level. From Hushmand et al [23].

A triangular distribution of dynamic pressure similar to the conventional M-O distribution (maximum pressure at the wall base) was measured on the most flexible structure. A more uniform pressure distribution with higher pressures was measured on the two stiffer structures. (See Figure 16 below.)

NEHRP Resource Paper Method

Studies on kinematic seismic earth pressures have been reported by Brandberg et al [24-27] and Durante et al [28,29]. Their work forms the basis of the recommendations in National Earthquake Hazard Reduction Program (NEHRP) Resource Paper 4, *Seismic Lateral Earth Pressures* [30]. It is stated in the Resource Paper that the recommendations are applicable to both free-standing retaining walls and restrained walls such as basement walls integral with the lateral force resisting system of the structure. The Resource Paper deals primarily with the kinematic component and does not provide details on how to include any inertial component.

The Resource Paper states that the kinematic component of interaction varies strongly with both the ratio of the wavelength, λ of an assumed vertically propagating shear wave to wall height, H and the relative wall-soil flexibility. An analysis method based on these parameters was developed that can be applied rigorously with a full response history or in a simplified manner that gives the peak response estimated from ground motion intensity. The simplified approach is described in the Resource Paper, and in Durante et al [29]. The method gives estimates of the seismic earth pressures force P_E and its point of application, h calculated using the following steps:

1. Perform seismic hazard analysis (probabilistic or deterministic) to estimate a design-basis peak ground velocity (*PGV)* for the site.
2. From the hazard analysis obtain the controlling magnitude and distance and estimate the mean period T_m. This period can be estimated using Figure 6 below. Compute the corresponding angular frequency, $\omega = 2\pi/T_m$
3. Develop a shear wave velocity profile for the retained backfill soil and compute the time-averaged shear wave velocity over the wall height V_{sav}.

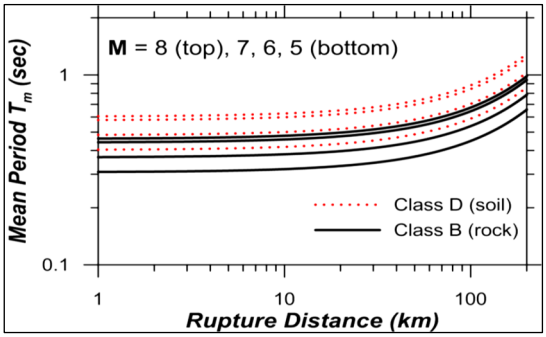

Figure 6: Mean period from Magnitude and distance. From Durante et al [29].

4. Estimate the ground surface displacement using the following equation and adjustment factor, f_u. (The adjustment factor has been calibrated to match the results of single-frequency analyses to more complete Fourier series analyses, Brandenberg et al [24]):

$$u_{g0} = \frac{f_u PGV}{\omega_m} \tag{1}$$

f_u is plotted in Figure 8 (a) below.

5. Calculate the static stiffness intensity k^i_{yo} from the following equation. This is based on the assumption of a rigid vertical wall supported on a rigid foundation. The stiffness intensity is the translational stiffness divided by the wall area.

$$k^i_{y0} = \frac{\pi}{\sqrt{(1-\nu)(2-\nu)}} \frac{G}{H} \tag{2}$$

where G is the average shear modulus over the height of the wall and ν the Poisson ratio.

6. Compute the ratio of the backfill soil stiffness to the wall stiffness β using the following equation. In cases where the wall section has not been determined an initial estimate of βH in the range of 1-2 can be applied and will often be conservative.

$$\beta = \sqrt[4]{\frac{k^i_{y0}}{4\,EI}} \tag{3}$$

where E is the Young's modulus for the wall material and I the moment of inertia of the wall section. β has units of L^{-1}.

7. Compute (equations are given in the Resource Paper) the normalized force amplitude $\overline{P_{E,Rigid}} = P_E/(k^i_{yo}\, u_{g0}\, H)$ and the resultant height h/H for a rigid wall. These quantities are shown in Figure 7. The wavelength ratio $\lambda/H = V_{sav}\, T_m/H$.

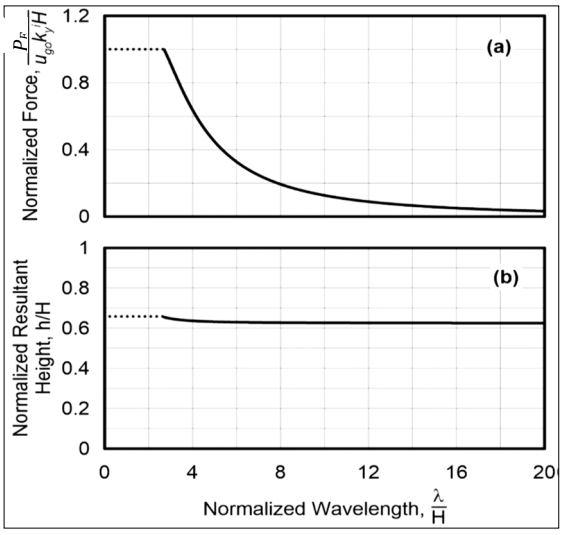

Figure 7: (a) Normalised force and (b) height of action for rigid wall. From NEHRP Resource Paper [30].

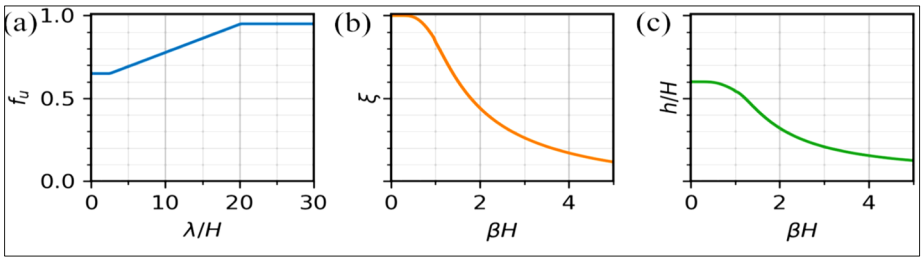

Figure 8: (a) Ground motion amplitude adjustment factor; (b) Stiffness reduction factor for wall force; (c) Force effective height. From Durante et al [29].

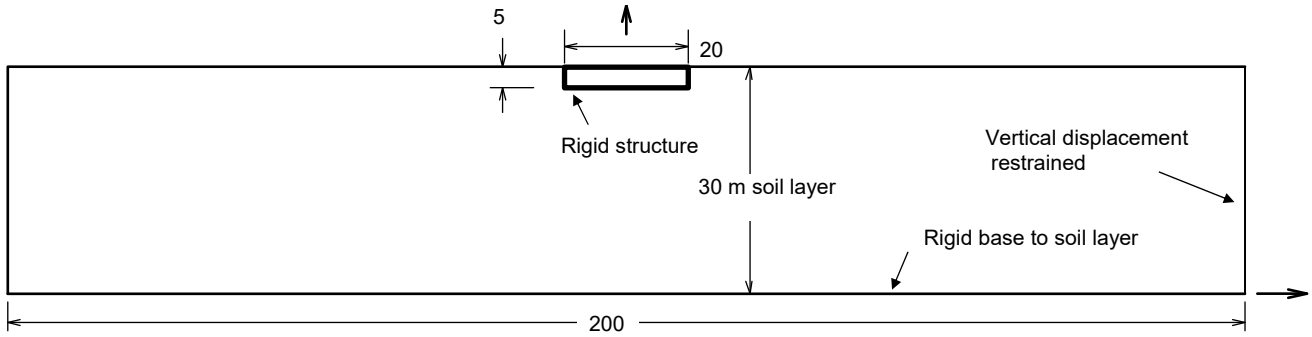

Figure 9: FEA model for illustrating dynamic interaction.

8. Adjust the rigid wall force and height of action for wall flexibility using Figure 8 (b) and (c). ξ is the ratio of the rigid wall force to the force on the flexible wall. (Equations are given in the Resource Paper.)
9. Compute the actual force and resultant height from the normalised values using the stiffness and ground displacement values k^i_{yo} , u_{g0} and the wall height H. The actual force P_E is given by:

$$P_E = \overline{P_E} k^i_{y0}\, u_{g0}\, H \qquad (4)$$

Comments on Resource Paper Method

The basis of the Resource Paper method is the assumption that the interaction of the wall with the soil can be modelled by horizontal Winkler springs on the face of the wall. This results in the dynamic forces on the wall being sensitive to the wavelength assumed for vertically propagating shear waves in the soil layer. Basement structures have significant lateral extent and the interaction with the soil is more complex that can be modelled satisfactorily with Winkler springs. As part of the present study the influence of the soil layer wavelength on the forces generated on basement walls was investigated using a two-dimensional elastic FEA to calculate the first mode dynamic response of a uniform 30 m deep by 200 m long soil layer incorporating a rigid massless basement block 20 m long by 5 m deep embedded in the layer at the horizontal centre of the layer. A schematic layout of the FEA model is illustrated in Figure 9.

The end boundaries of the layer were taken to be unrestrained horizontally but restrained against vertical displacement. Ten 0.5 x 0.5 m elements were used over the height of the wall. The shear modulus of the layer was taken as 60 MPa and the soil density as 1.8 t/m^3.

Contours of displacement recorded in millimetres close to the wall in the first mode response of the layer scaled to a free field acceleration of 1 g are shown in Figure 10. The rigid block interaction with the soil forces the displacements in the soil layer near the wall to become relatively uniform over the height of the wall.

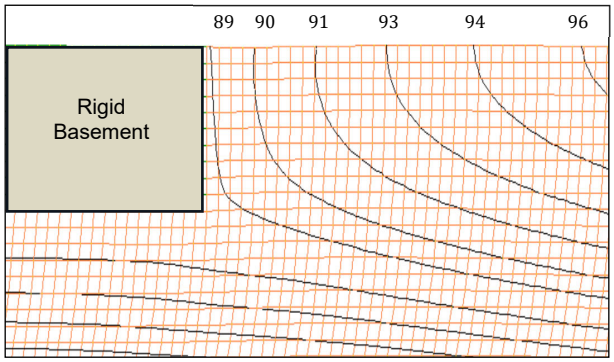

Figure 10: Contours of displacement (mm) in first mode response.

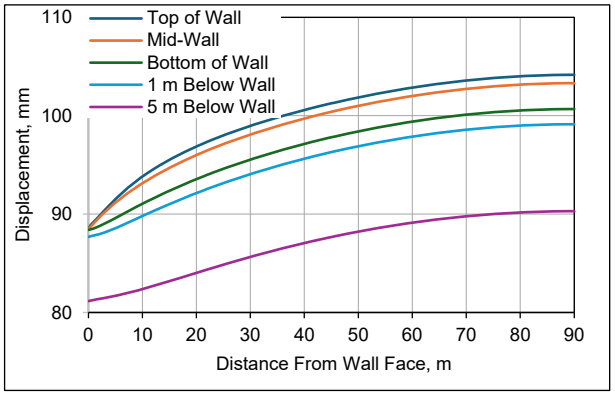

Figure 11: Displacement variation with horizontal distance from the wall.

The variation of displacement with distance from the wall face is shown in Figure 11 for various heights on the wall and below the wall. From these displacements it is clear that the interaction of the block in the soil layer has a marked influence on displacements for significant distances below the soil surface and laterally from the wall face. This displacement behaviour is

also influenced by the width of the basement structure (see Figure 18 below) and cannot be well represented with Winkler springs.

From the Theory of Elasticity (Timoshenko and Goodier [31]) the horizontal stress in the soil elements, σ_x can be estimated from the following plane strain stress-strain relations:

$$\frac{\sigma_x}{G} = m^2 \frac{\partial u}{\partial x} + (m^2 - 2)\frac{\partial v}{\partial y} \quad (5)$$

where u and v are the horizontal and vertical displacements respectively, and $m^2 = \frac{2(1-\nu)}{(1-2\nu)}$ where ν = Poisson ratio.

Since the variation of the vertical displacement is small the horizontal stress is given approximately by:

$$\frac{\sigma_x}{G} = m^2 \frac{\partial u}{\partial x} \quad (6)$$

The slope of the displacement curves shown in Figure 11 near the wall therefore indicate significant horizontal pressure on the wall with the highest values near the top of the wall. The Winkler spring assumption used in the Resource Paper method may not accurately model this rate of change of horizontal displacement near the wall.

The pressure on the wall was calculated by the FEA and is shown in dimensionless form in Figure 12. The pressure has been scaled to a 1 g acceleration in the free-field (FF) on the ground surface. Integration of the pressure distribution gives a dimensionless force ($P/\gamma H^2$, where γ is the soil unit weight and H the wall height) of 1.14 for a 1 g free-field acceleration which of the same order as indicated in previous studies of rigid walls subjected to static horizontal ground motions (Wood, [13]).

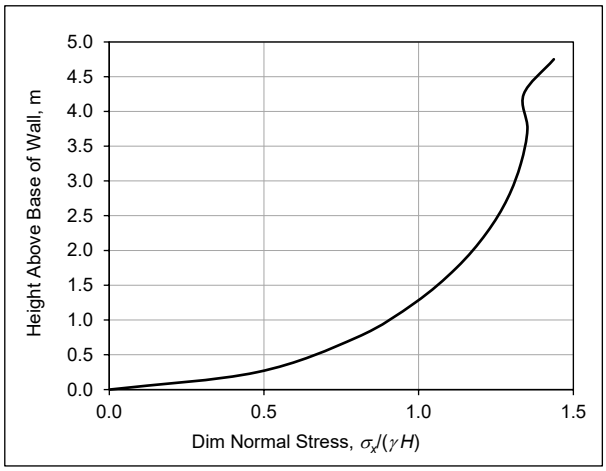

Figure 12: Pressure on wall of rigid block.

The Resource Paper calculation method was applied to this rigid basement structure to determine the earthquake force and its height of application. The steps using this method were:

- The PGV was assumed to be the FEA value of 1.01 m/s scaled to a free-field acceleration of 1 g.
- The mean period was taken from the FEA analysis which gave a value of 0.65 seconds, This value was consistent with Figure 6 assuming strong shaking on a soil layer from a Magnitude 7 or greater event. The angular frequency calculated from the FEA period was 9.7 rad/s.
- A shear wave velocity of 183 m/s over the wall height was calculated from the assumed shear modulus and the soil density.
- The peak ground surface displacement was calculated using Equation (1) with f_u estimated from Figure 8(a) and using $\lambda/H = V_{sav}\, T_m/H = 23.6$. This gave a displacement of 99 mm.
- The static stiffness intensity was calculated using Equation (2) which gave a value of 34.6 MN/m^3.
- The wall was assumed to be rigid so no stiffness reduction was computed.
- The normalised force amplitude was computed using the following wavelength reduction factor equation used to generate Figure 7:

$$\frac{P_E}{k^i_{yo} u_{go} H} = \frac{\sin(kH)}{kH} - \cos(kH) \quad (7)$$

where, $kH = 2\pi H/\lambda$

This gave a normalised force amplitude of 0.023.

- Using Equation (4) the actual force on the wall, P_E was calculated to be 400 kN/m and the resultant height ratio estimated from Figure 7 was 0.63. The dimensionless force ($P_E/\gamma H^2$) was computed to be 0.91.

This dimensionless force is significantly less than the equivalent force on the wall calculated directly by the FEA of 1.14. The FEA gave the height ratio as 0.57 which is lower than the 0.63 value computed by the Resource Paper method.

The Resource Paper method uses a soil-structure stiffness parameter β, which is based on the analysis of beams on an elastic foundations using Winkler springs (Pender [32]). Although appropriate for the assessment of the interaction of a simple wall structure with the adjacent soil it does not account for any difference between the roof and floor displacement of a flexible basement structure having substantial lateral width. This limitation is illustrated by investigating the displacements of the Hushmand et al [23] Base Line (BL) reservoir box structure subjected to the Northridge-M input motion with a PGA of 0.81g in their Test 1A. (The Hushmand et al tests were used in the Resource Paper to verify the method.) The βH value based on the concrete box wall moment of inertia and Young's modulus was estimated to be 1.6 and from Figure 8(b) the force reduction from a rigid wall for this flexibility factor is 0.6. Insufficient information on the soil response was published by Hushmand et al to apply the Resource Paper method in detail but on the assumption of an average shear modulus of the soil layer of 20 MPa over the height of the wall and a wavelength based on a T_m of 0.65 seconds the wall force based on a rigid assumption was estimated to be 1,400 kN/m. Allowing for the flexibility reduction of 0.6 the wall force reduces to approximately 800 kN/m or in dimensionless form ($P/\gamma H^2$) a force of 0.45. Reducing the shear modulus to a likely lower limit of 10 MPa increases the dimensionless force to 0.49 and reducing T_m to a lower limit of 0.5 seconds increases the dimensionless force by a significant amount to 0.74. The recorded experimental dimensionless force was 0.29 indicating a significantly more flexible structure than computed from the βH value. In the Resource Paper a comparison between the Resource Paper method and the Hushmand et al Test 1A results showed that the test results were overestimated by the proposed analysis method.

The deflected shape of the Hushmand et al BL reservoir model computed by a FEA in the present study for the Northridge-M input motion is shown in Figure 13 and indicates that the overall "shearing" deformation is much greater than the local deflection of the wall beam section between the top and bottom of the box suggesting that a stiffness reduction based on a β parameter for the wall is not appropriate for this structure. The "shearing" deformation arises mainly from rotation of the wall at the joint with the floor slab which has was 0.69 m thick. The wall thickness was 0.56 m and this resulted in the floor being

moderately flexible in relation to the floor (flexural stiffness approximately 1.6 greater than the walls).

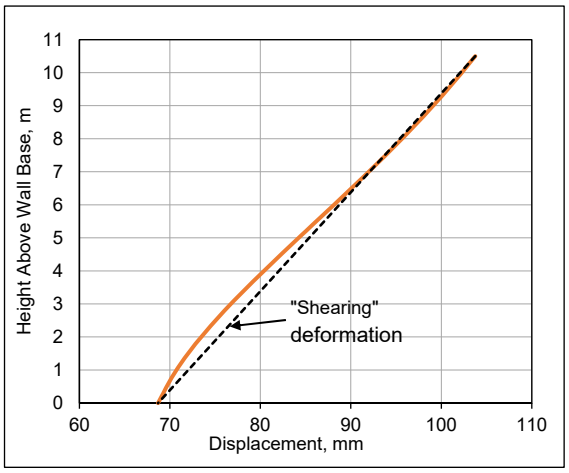

Figure 13: Deflection of wall of Hushmand et al BL model in the Northridge-M input ground motion.

ELASTIC FEA STUDY

The review of published research on earthquake pressures on basement walls showed that the commonly accepted and recently proposed methods gave very large variations in the earthquake kinematic pressure component. The Ostadan [11] method typically gave pressures approaching those expected on rigid walls located on a stiff foundation whilst the Taiebat et al [14] pressures based on reduced M-O pressures were much lower. Some of the centrifuge results also gave unexpectedly low pressures although the direct dynamic pressure measurements made by Hushmand et al [23] on model reservoir structures with similar stiffnesses to typical basement walls were higher than indicated by other tests. To explore these differences a study using elastic two-dimensional FEA methods was instigated. Initially the models used in the centrifuge studies were investigated. The work was extended to consider both the kinematic and inertia pressure components on basements of varying geometry and stiffness. Finally, the earthquake induced basement wall pressures were calculated for a 7-storey steel framed building supported on piles with a basement depth of 3.3 m. Results of the present study are summarised in the following sections.

Centrifuge Tests of Wagner & Sitar

The 13.3 m deep centrifuge model basement investigated by Wagner and Sitar [20] and shown schematically in Figure 3 was analysed using the elastic FEA method. A uniform fine mesh of 0.1 x 0.1 m was used for both the structure and walls. This was easy to generate and results in modest compute times. Both static analyses using a uniform horizontal body force and dynamic modal analyses were carried out.

The walls of the model were 0.47 m thick in prototype scale and constructed of aluminium alloy. They were stiffened with vertical ribs and in the two-dimensional FEA model assumed to have a uniform thickness of 0.7 m to give a similar moment of inertia to the model. The wall footings were 2.7 m wide and 0.9 m deep. Soil boundaries at the left and right of the model were assumed restrained in the vertical and free in the horizontal direction. The soil in the elastic FEA was assumed to be uniform over the height of the model and founding soil with a shear modulus of 18.8 MPa and a Poisson ratio, ν of 0.33 (Young's modulus of 50 MPa). Soil pressures on the wall are not very sensitive to these values but are affected by any variation in the elastic constants over the depth of the model. Under the 0.5 g earthquake load used in the analysis (uniform body force for the static analysis and free-field acceleration on the ground surface in the dynamic analysis) tension pressures occur near the top of the walls. A gap of depth 1.8 m was assumed to approximately model this effect. Below this depth the gravity soil pressures will prevent significant tension pressures at the wall face.

Pressure distributions calculated by the elastic FEA's are shown in Figure 14. The dynamic pressure component was computed using only the first mode response (frequency of 1.48 Hz). In one dynamic case the free-field acceleration on the soil surface at the soil end boundaries was used to calculate the response and in the other the average acceleration over the height of the wall. This later procedure gives good agreement with the static analysis based on a uniform 0.5 g body force.

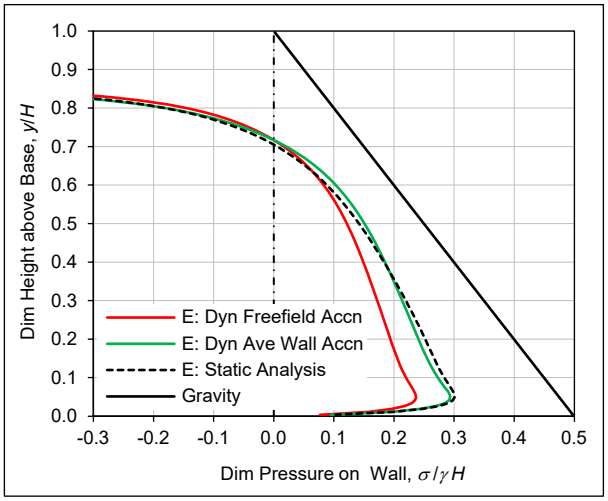

Figure 14: Pressures from elastic FEA.

The earthquake pressure components are not similar in shape to the experimental and numerical pressures shown in Figure 4 (reproduced from Wagner and Sitar [20]; the earthquake input motion had an average ground surface PGA of 0.5 g). The elastic FEA pressures were strongly influenced by rotation of the basement walls about their base and a reason for the difference could be related to the stiffness of the cross beams which affect this rotation. They may have been stiffer in the centrifuge model than assumed in the elastic FEA.

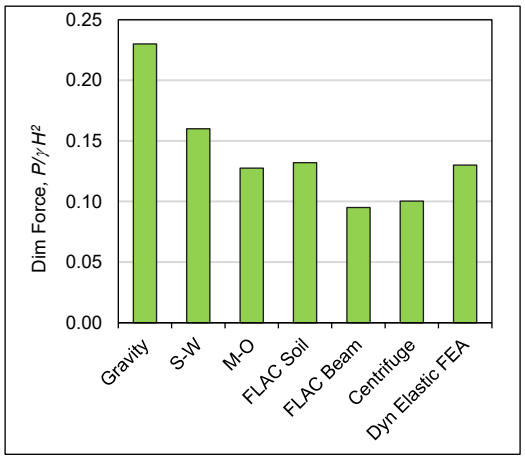

Figure 15: Forces on wall from various earthquake analyses and gravity.

Force components obtained by integrating the pressure distributions shown in Figures 4 and 14 are shown in Figure 15. Although the pressure distributions are not very similar there is reasonable agreement between the earthquake force from the soil mesh pressures in the Wagner and Sitar FLAC analysis and the elastic FEA of the present study. For comparison, the

dimensionless earthquake force ($P/\gamma H^2$ - where P is the force per unit length of wall) from a 0.5 g static body force acceleration acting on a rigid smooth wall supported on a rigid foundation is 0.49 indicating that the Wagner and Sitar basement wall was very flexible.

Centrifuge Tests of Hushmand et al.

The intermediate stiffness reservoir model (BL model) used by Hushmand et al. [23] in their experimental centrifuge study was analysed using the elastic FEA method described above. Figure 5 shows the schematic layout of the centrifuge model and a similar structure-soil layout was used in the FEA. In prototype scale the reservoir thicknesses of the roof, walls and floor were 0.4, 0.6 and 0.7 m respectively. The overall height and widths of the structure were 10.5 and 12.2 m respectively. The depth of the soil layer below the structure was 8.2 m and the distance of the soil end boundaries from either side of the structure was 14.9 m. Both a uniform soil with a shear modulus of 18.8 MPa and non-uniform soil with this modulus varying from 15 MPa at the surface to 22.6 MPa at the base were used. The Poisson ratio for both soil types was taken as 0.33. The soil was assumed to be in bonded contact over the complete height of the walls.

Figure 16 compares the earthquake pressures from one of the centrifuge experiments (Northridge-M input record) with the pressures calculated for the first mode response in the elastic FEA using the same free-field ground surface PGA of 0.81 g. The FEA results are for the non-uniform soil and show good agreement with the experimental pressures over most of the wall height.

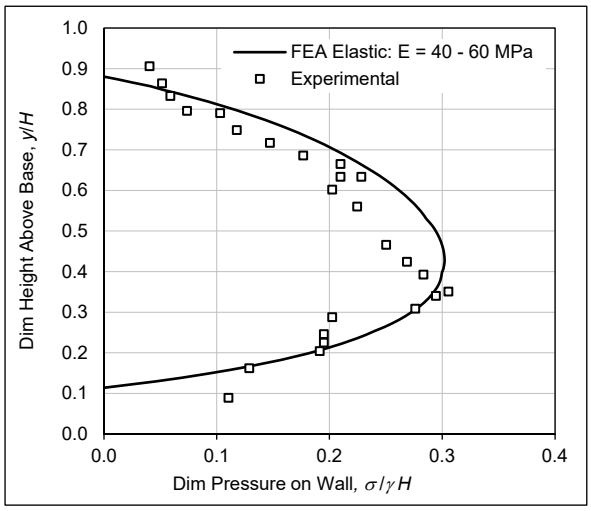

Figure 16: Pressures from Hushmand et al. [23] intermediate stiffness BL model.

Wall Force from Soil Layer Response

A number of plane strain elastic FEA's were carried out to investigate the main parameters that influence the pressure force on basement walls from both the shear deformations in the soil generated by the earthquake waves (kinematic) and the movement of a wall against the soil (horizontal translation and rotation) resulting from the inertia forces acting on the building above basement level. The analyses to determine the pressures forces from the soil layer response are described in this section and the analyses carried out to determine forces from wall movements in the following section.

Basement structures of various horizontal stiffnesses with an overall depth of 5 m and horizontal widths of 5, 15 and 30 m were analysed. In addition, a 10 m width was used for the case of a fully rigid structure. The basements were modelled using box structures with 0.5 m thick plane-strain beam elements (modelled as line elements). A single cell box was used for the 5 m wide structure and three and six cell structures for the 15 m and 30 m wide structures respectively. The beam elements were assumed to be massless.

The basement structures were embedded in soil layers of depths, 5, 10, 20, and 50 m with the top of the basement structure at the surface of the soil layer. The soil was modelled with plane-strain quadrilateral elements. Both a uniform soil layer with a shear modulus of 40 MPa and a variable stiffness layer with a shear modulus varying from 16 MPa at the surface to 64 MPa at a depth of 50 m (average of 40 MPa in the layer) were used. Both the uniform layer and variable stiffness layer had a Poisson ratio of 0.4 and a uniform mass density of 2 t/m^3. In the variable stiffness layer models for the 10 and 20 m depths the soil had a modulus that increased with depth at the same rate as used in the 50 m layer (0.96 MPa/m). For the 5 m soil layer (structure supported on rigid base) the variable stiffness soil layer had a shear modulus that increased from 16 MPa at the surface to 28 MPa at the base (rate of increase of 2.4 MPa/m). A mesh size of 0.0625 m x 0.0625 m was used in the vicinity of the structures giving 80 elements over the height of the basement. Symmetry was used on the structure horizontal centreline to reduce the size of the analysis model. The soil layer extended 100 m from the centreline of the structures and the layer boundary remote from the structures was restrained vertically but allowed to displace horizontally.

The geometry for the 5, 15 and 30 m wide structures and embedding soil layers are shown in Figure 17. When supported on pins at the column-base joints the horizontal shear stiffness for load applied at roof level of the single cell box structure with an equal height and width of H, and the line element members having a thickness, t and Young's Modulus, E is given by:

$$K_b = 12E\left(\frac{t}{H}\right)^3 \tag{8}$$

Approximate stiffnesses for multi-cell boxes can be obtained by summing the individual stiffnesses of the columns, top and base members and then distributing these to a single cell. More correct shear stiffnesses were calculated for the three and six cell basement structures using a beam element FEA model. The stiffness of the box structures was varied by changing the E values.

For describing the stiffness of the structure in dimensionless terms a flexibility ratio, F_r was defined by:

$$F_r = \frac{Soil\ flexibility\ of\ free-standing\ structure\ without\ soil\ interaction}{Shear\ flexibility\ of\ soil\ block\ of\ same\ overall\ dimensions\ as\ structure} = \frac{f_{st}}{f_s} \tag{9}$$

Soil shear stiffness is defined by:

$$K_s = G = \frac{\tau}{\gamma} \tag{10}$$

where: G = soil shear modulus in the soil over the level under consideration, τ = soil shear stress and γ = soil shear strain.

From the soil shear stiffness definition, the shear flexibility of a block of soil of height H and length L is given by:

$$f_s = \frac{H}{LG} \tag{11}$$

For the analyses with the shear modulus varying over the height of the soil layer the average G over the height of the basement wall was used to define the structure flexibility ratio.

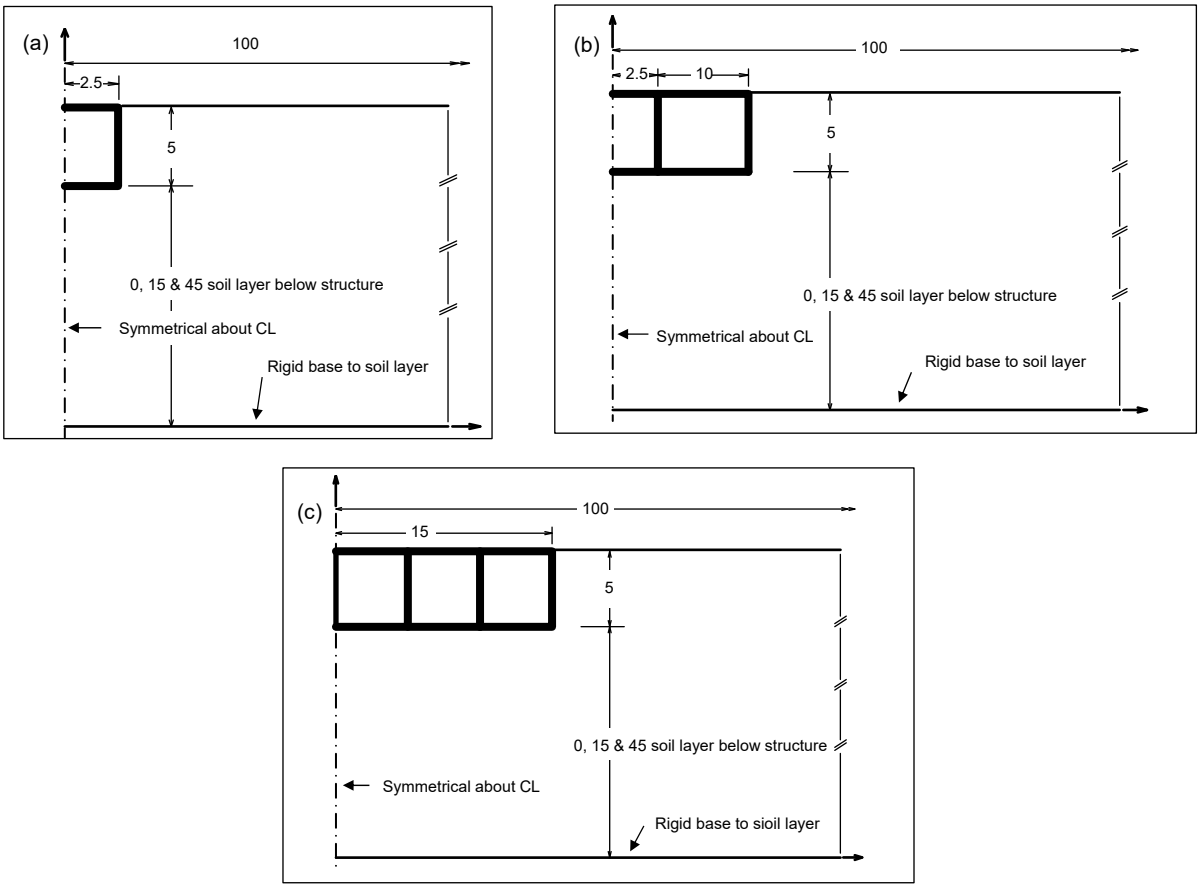

Figure 17: Geometry of basement wall models. (a) 5 m width, (b) 15 m width and (c) 30 m width.

Both static and dynamic analyses were carried out on the basement/soil layer models. In the dynamic analyses the first horizontal mode of vibration was computed and this mode scaled to give a 1 g free-field acceleration at the top of the soil layer 100 m from the structure centreline. In this first mode the soil layer deforms mainly in shear and the response therefore simulates the vertical propagation of a shear wave. In the static analysis a uniform 1 g body force was applied to the soil layer.

Soil pressure forces calculated for the wall of a rigid structure are shown in Figure 18 as a function of the width of the basement structure embedded in uniform soil layers of total depths 20 and 50 m. The pressure force per unit length of wall, P for a 1 g body force (static) or 1 g free-field acceleration (dynamic) is plotted in dimensionless form ($P/\gamma H^2$). Both the dynamic and static analyses results are shown for the 20 m layer. For the 50 m layer the dynamic and static forces agreed within 2%. The results show that the pressure force is sensitive to the width of the basement structure. The wider structures rotate less and are stiffer for horizontal loading because of the larger shear resistance of the soil on their bases.

The dynamic loading pressure distributions normal to the walls of 5, 10, 20 and 30 m wide rigid basement structures embedded in the 20 m deep soil layer are shown for the 1 g free-field acceleration in Figure 19. The centre of pressure height above the base varied between 0.55 to 0.61 H.

Dynamic loading pressure distributions on a 20 m wide rigid basement embedded in a 50 m deep layer with uniform, 16 to 64 and 0 to 300 MPa soil shear modulus variations are shown in Figure 20.

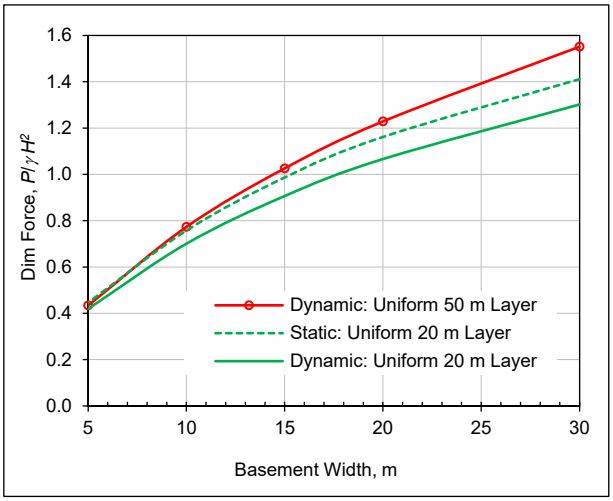

Figure 18: Pressure forces on rigid basement structures.

Soil pressure forces calculated on the wall of a 5 m wide flexible basement structure are shown in Figure 21 as a function of the structure flexibility ratio for soil layer depth, D to wall height H ratios (D/H) of 10, 4, 2 and 1. Forces for both the uniform and variable modulus layers are shown. The results are from the dynamic analyses (first mode) scaled to 1 g free-field acceleration and show that the pressure force is not very sensitive to the structure flexibility and only moderately sensitive to the soil modulus variation in the soil layer. For D/H from 2 to 10 the force is not strongly influenced by this ratio. As the D/H ratio increases the transfer of the shear stresses from the structure to the boundary decreases and this reduces the shear force on the base of the structure leading to greater forces on the vertical wall structure. There is a significant drop in the

force between D/H values of 2 and 1. A D/H of 1 is corresponds to the case of both the wall and layer on a rigid base. Wood [13] showed that for a static 1 g body force this "rigid wall" case results in a dimensionless wall force of approximately 0.9. Contrary to expectation the first mode (1 g FF) dynamic dimensionless pressure force is much lower at approximately 0.12.

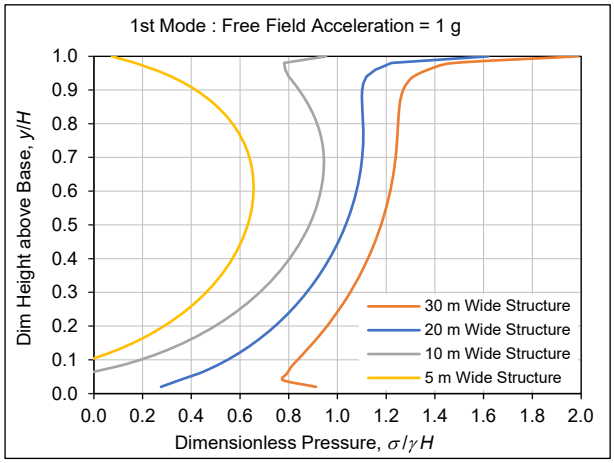

Figure 19: Pressures on rigid basement, 20 m layer.

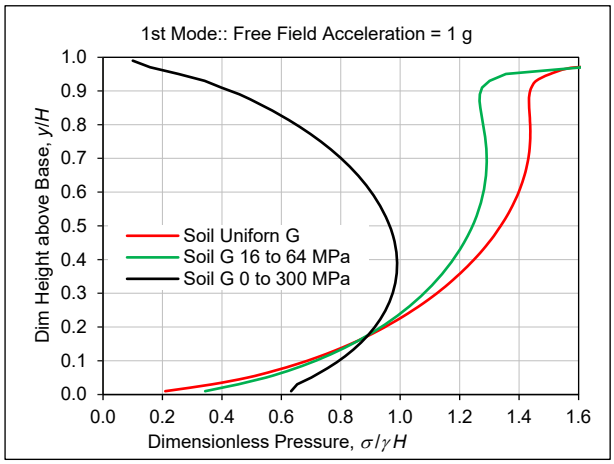

Figure 20: Pressures on rigid basement, 50 m layer.

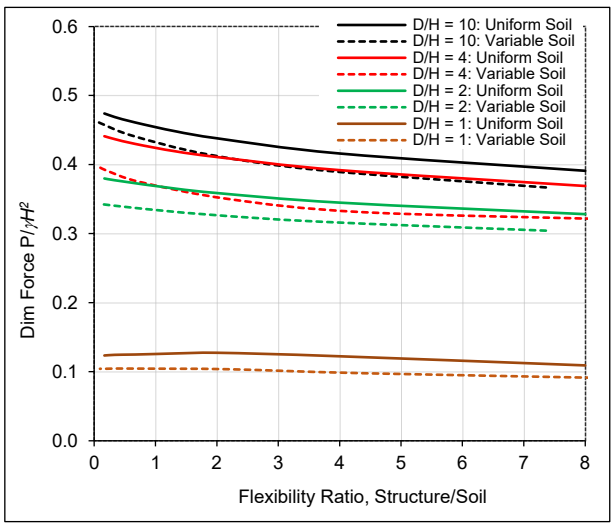

Figure 21: Forces on 5 m wide basement. 1 g FF.

In the dynamic case the first mode shape is affected by the rigid base near the wall resulting in reduced displacements and inertia forces in the soil. Pressures calculated for a rigid wall on a rigid base by analyses for the 1st Mode dynamic and the static 1 g body force are compared in Figure 22. Also shown is the pressure computed by adding a large number of modal components by the Square Root of the Sum of the Squares method (SRSS) and the absolute sum of the modes. For this comparison the modal components including the 1st mode were calculated for a spectral acceleration of 1 g. (The free-field accelerations are not scaled to 1 g for this case.) The absolute sum of the complete set of modal components should add to the static pressure for this uniform 1 g spectral response. This comparison again shows that a dynamic analysis for the rigid wall on a rigid base gives much lower pressures than calculated by the static body force analysis. (Figure 22 pressures are based on FEA's using a mesh with 10 elements over the height of the wall.)

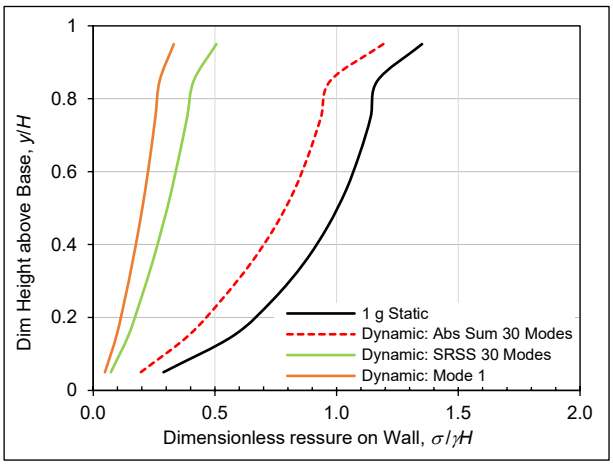

Figure 22: Pressures on rigid wall on a rigid base. Bonded contact.

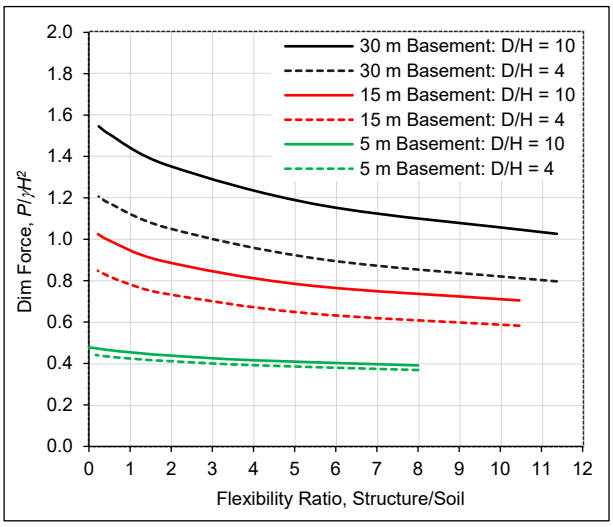

Figure 23: Force on flexible basement wall: uniform soil.

Soil pressure forces calculated for the wall of 5, 15 and 30 m wide basement structures are shown in Figure 23 as a function of the structure flexibility ratio for soil layer depth to wall height ratios of D/H of 10, and 4. Figure 24 compares the pressures for uniform and variable soil stiffness layers on the three basement widths for a D/H of 10. As was the case for the rigid structures the pressure force is sensitive to the width of the basement structure. For the 30 m wide structure both the depth ratio D/H and the flexibility ratio have a moderate influence on the force on the wall. These ratios have less influence on the narrower 5 and 15 m wide structures. The soil layer with stiffness variability reduces the pressures on the 30 m wide

basement by about 15% but has less influence on the 15 and 5 m wide structures.

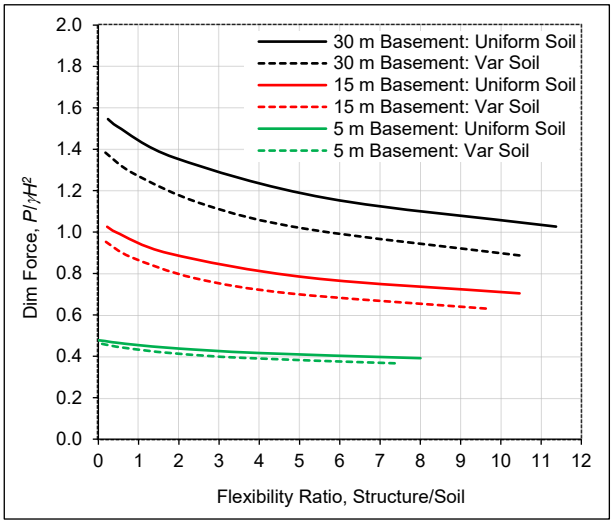

Figure 24: Force on flexible basement wall for D/H = 10.

The pressure forces shown in Figures 23 and 24 indicate that when the width of the basement is greater than approximately three times its height ($B/H > 3$, where B is the width) the dimensionless pressure force for a 1 g free-field acceleration will be greater than 0.6 regardless of the flexibility ratio or shear stiffness of the structure (horizontal load at the basement roof level). For structures with $B/H > 6$ and low flexibility ratios the dimensionless force under a 1 g free-field acceleration may exceed 1.5. This force level is significantly higher than estimated for a rigid wall on a rigid foundation loaded by a static 1 g body force in the soil layer (see Figure 22).

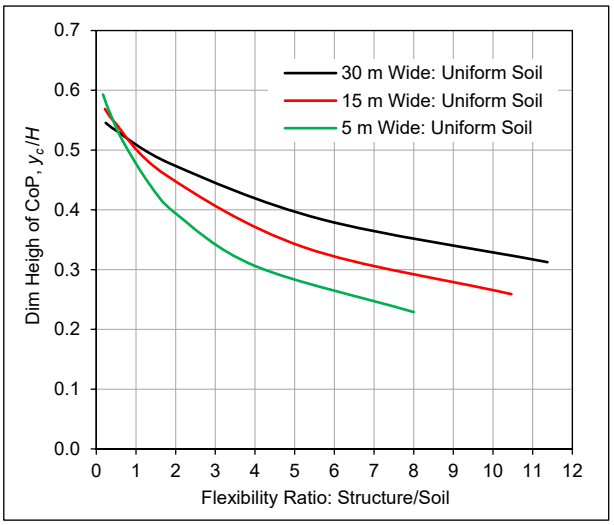

Figure 25: Centre of pressure ratio for flexible basement walls.

The centre of pressure (CoP) ratios, y_c/H where y_c is the height of the CoP above the base, versus the flexibility ratio calculated for the earthquake forces on the walls of flexible basements with widths of 5, 15 and 30 m are shown in Figure 25. The CoPs are based on a 50 m deep uniform layer for the 15 and 30 m wide basements and a 10 m uniform layer for the 5 m wide basement. For layer depth ratios of $D/H > 2$ the layer depth does not have a significant effect on the CoP ratio. Results for the layers with a variable soil modulus differed by less than 2% from the uniform soil values. The CoP ratios ranged from 0.6 for rigid basements to 0.23 for basements that very flexible under shear deformation loading. Basements of narrow width rotate significantly and this reduces the CoP height ratio.

As mentioned above, Hushmand et al [23] carried out centrifuge model tests on a number of concrete reservoir structures. Three of the tests were carried out using cohesionless soil with the reservoir roof at the surface of level ground (similar to a basement wall). A schematic layout of the centrifuge model and soil layer used in these tests is shown in Figure 5. Each of the three tests was on a structure of differing flexibility. The overall height and widths of the structure were 10.5 and 12.2 m respectively giving a $B/H = 0.9$. The depth of the soil layer was 18.7 m giving $D/H = 1.8$ and the distance of the soil end boundaries from either side of the structure was 14.9 m. Geometric ratios for the model therefore were similar to those used in the FEA's carried out for the 5 m wide structure embedded in a 10 m soil layer ($B/H = 1.0$ and $D/H = 2.0$). Figure 26 compares the maximum dynamic forces recorded in the Hushmand et al experiments with the FEA results from the present study for these geometric ratios.

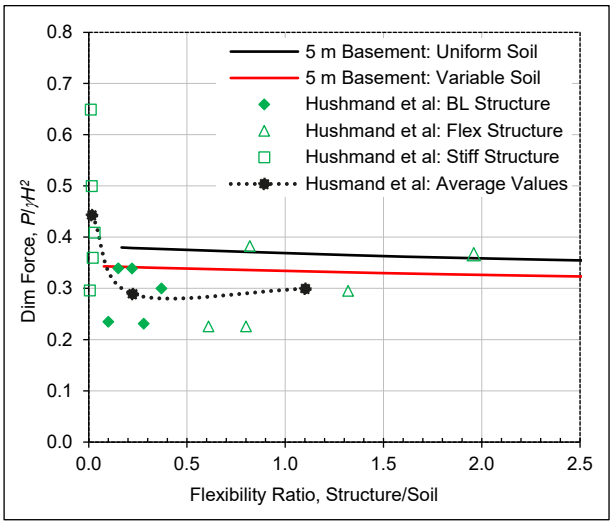

Figure 26: Comparison of experimental forces with FEA for 5 m wide structure in 10 m deep layer.

The Hushmand et al flexibility ratios and dynamic forces were scaled from figures in their paper (Figures 4-9 and 4-15). Their flexibility ratios were based on measured stiffness values for the structure but details of how the soil moduli were estimated were not presented. Free-field accelerations recorded in the experiments were given as 0.3 to 1.0 g. The reported experimental flexibility ratios correspond to a soil shear modulus of between 3 to 11 MPa. These relatively low values and the high recorded accelerations suggest that significant nonlinear response was likely in the soil layer over the height of the structure.

To compare the experimental results shown in Figure 26 with the dynamic forces predicted by the present study the experimental results were scaled to a free-field acceleration of 1 g. Although there was significant scatter in the experimental forces the average values for the three individual structures show moderately good agreement with the forces predicted by the present study. The stiff structure experiments indicated higher forces than predicted but the BL and flexible structures indicated rather lower forces. Overall, the stiffness of the structure did not have a major influence on the experimental dynamic forces.

Superstructure Inertia Loads

To investigate the forces generated on basement walls from displacements arising from the superstructure inertia loads applied to the basement structure, elastic two-dimensional

FEA's were carried out on a rigid basement structure of width 20 m and height 5 m subjected separately to both horizontal translation and rotation displacement about the transverse horizontal centre-line. In a number of analyses the horizontal and rotational displacements were applied directly and in other cases forces were applied to generate uniform horizontal displacements or rotation. This latter method was used in the final part of the study to provide overall stiffness values that could be verified by comparison with analytical results.

The basement structures were embedded in soil layers of depths 20 m and 50 m with the top of the basement structure at the surface of the soil layer. The soil layer was modelled with plane-strain quadrilateral elements and three different stiffness distributions were used: a uniform soil layer with a shear modulus of 19 MPa (Young's modulus of 50 MPa); in the 50 m layers a shear modulus increasing linearly from 14 MPa at the surface to 64 MPa at the base, and a shear modulus of zero at the surface increasing linearly to 300 MPa at the base. For the 20 m deep variable stiffness layers the shear modulus increased linearly from 14 MPa at the surface to 56 MPa at the base, and zero at the surface to 140 MPa at the base. In all the soil layers the Poisson ratio was taken as 0.3 and the mass density as 2 t/m^3.

In most of the analyses the full 20 m wide structure was modelled but initially a half width was modelled using symmetry about its vertical centre line. The finite element mesh was extended 50 m either side of the structure vertical centre line with the end boundaries taken as restrained against vertical displacement, but free in the horizontal direction and for rotation about the axis parallel with the wall surface. A 0.1 by 0.1 m mesh size was used giving 50 elements over the height of the wall. Basement walls with both bonded and smooth contact with the soil layer were investigated. The smooth contact was modelled using rigid pinned links between the soil and wall. A schematic of the FEA model geometry is shown in Figure 27.

The pressure distributions normal to the wall computed for smooth and bonded walls subjected to translation and rotation displacements of the basement in both 20 and 50 m uniform soil layers are shown in Figures 28 (a) and (b). The wall height in the plots is plotted as the ratio y/H where y is the height above the wall base and H the height of the wall. Pressures, σ are expressed in dimensionless form for the translation case by multiplying by H and dividing by Eu, where E is the Youngs modulus at the base of the wall and u is the horizontal displacement, and for the rotation case by dividing by $E\theta$ where θ is the rotation about the base of the wall.

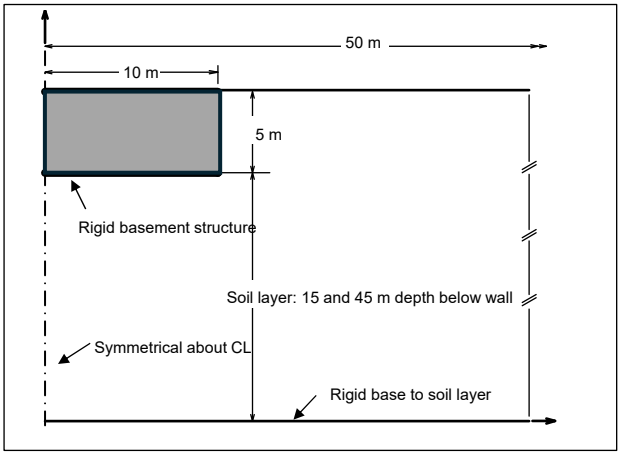

Figure 27: Rigid basement for superstructure inertia load analysis.

There are only minor differences between the pressures calculated for the bonded and smooth walls. Because of the elastic soil assumption, the translation displacement gives a high stress at the top of the wall but this would not be the case for typical soils which would become nonlinear or have a low modulus in this region. The soil layer depth affects the pressures for translation with the 20 m layer resulting in an effectively stiffer structure than for the 50 m layer depth. The difference in wall rotation pressures arising from the layer depth variation is relatively minor but pressures for the deeper layer are greater near the top of the wall.

Pressures on smooth walls embedded in the 20 m deep soil layer are compared for the three soil layer modulus distributions in Figures 29 (a) and (b). Corresponding pressure distributions for the 50 m deep layer are shown in Figures 30 (a) and (b).

The dimensionless force per unit length on the translating and rotating walls embedded in both the 20 m and 50 m deep soil layer are compared for the three soil layer modulus variations in Figure 31. Corresponding height ratios for the centres of pressures, y_c/H are shown in Figure 32. The forces and centre of pressures have been taken as the average of the smooth and bonded contact cases and were computed by integration of the pressure distributions shown in Figures 28 to 30.

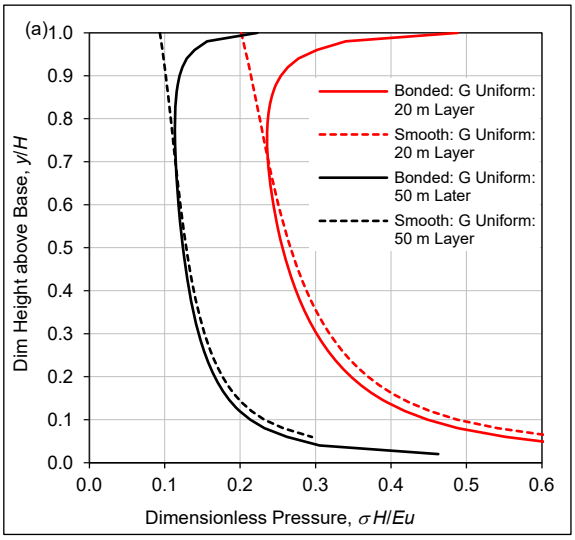

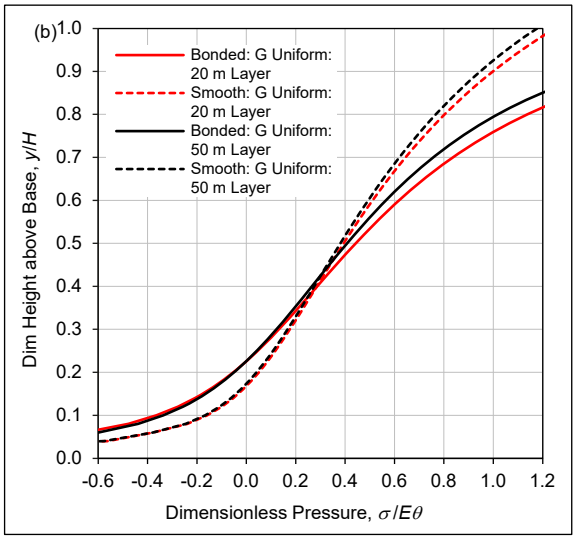

Figure 28: Pressures on rigid basement from (a) translation and (b) rotation.

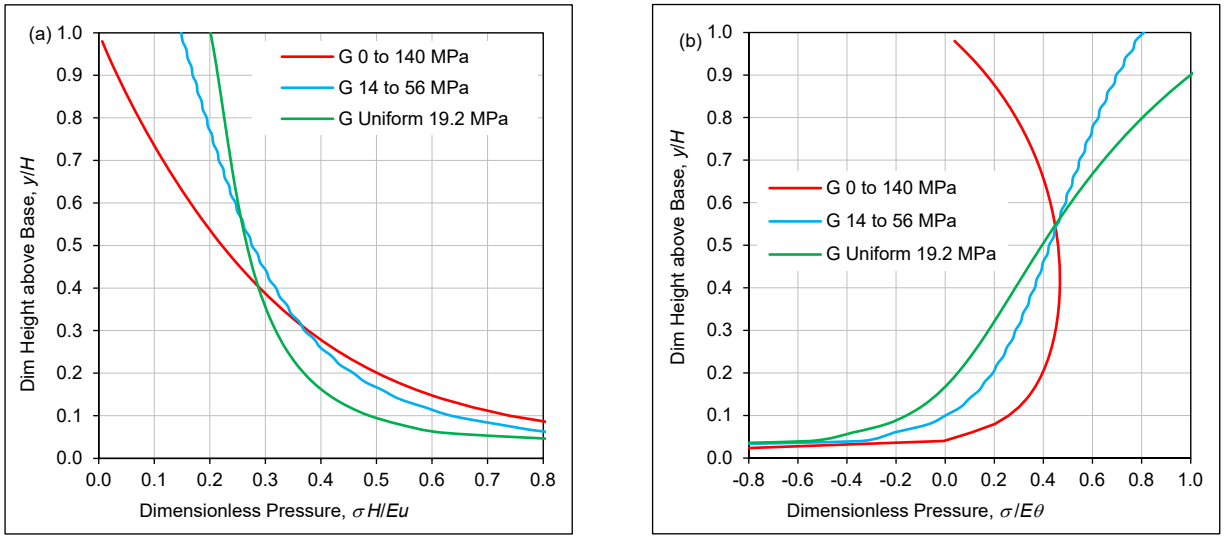

Figure 29: Pressures on rigid basement for 20 m layer from (a) translation and (b) rotation (smooth contact).

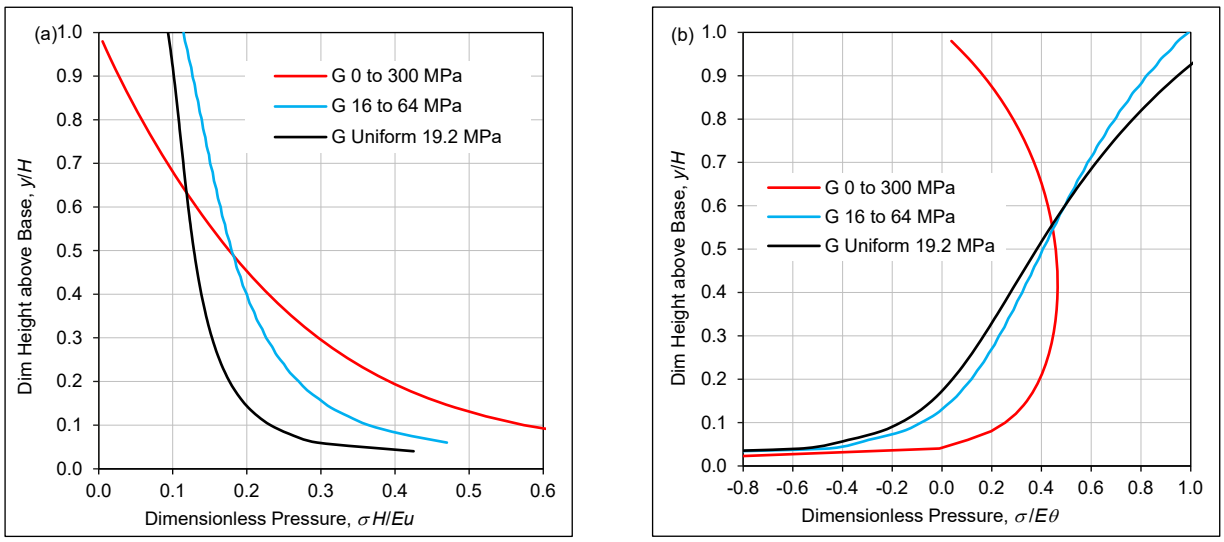

Figure 30: Pressures on rigid basement for 50 m layer from (a) translation and (b) rotation (smooth contact).

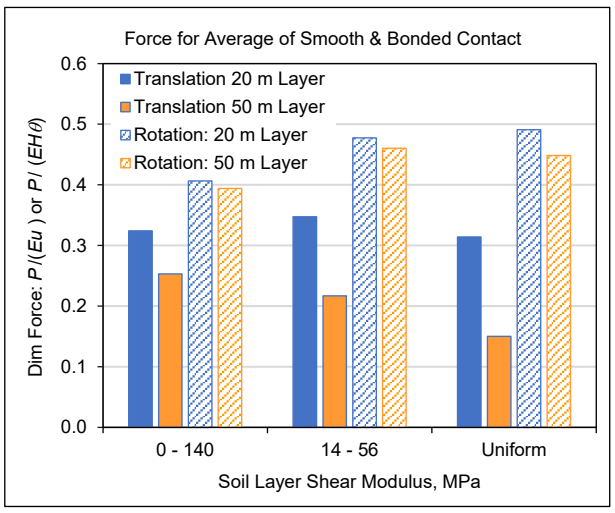

Figure 31: Force on rigid basement embedded in 20 and 50 m layers.

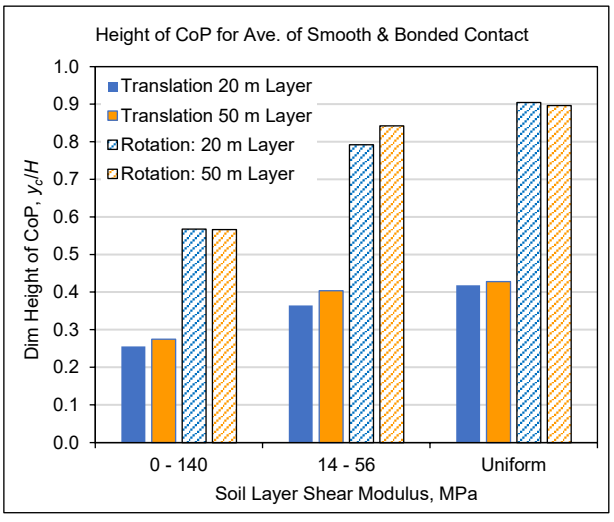

Figure 32: Centre of Pressures on rigid basement embedded in 20 and 50 m layers.

As indicated by the pressure distributions the wall forces for translation are sensitive to the layer depth and soil modulus variation. Forces and the centres of pressure from wall rotation are much less sensitive to the layer depth although the soil modulus variation has a moderate impact. The very high centre of pressures for the wall rotation are partly the result of the elastic soil assumption and would be lower for most soils encountered in practise if they have low modulus values or exhibit nonlinear response near the ground surface.

Stiffness of Basement Structure

To predict the displacements of a basement structure arising from the superstructure inertia loads applied at the top of the basement it is necessary to estimate both the horizontal and rotational stiffness of the basement structure. Many buildings will have pile foundations and if this is the case estimating the stiffness may require a structural analysis with the piles modelled by one of the recognised methods such as Winkler springs or elastic continuum (Pender [32]). For buildings on raft foundations there are several analytical solutions based on elastic soil assumptions that are helpful for preliminary analysis. Stiffness equations for a two-dimensional structure embedded in a uniform elastic soil layer are given by Jakub, [33] (also presented by Gazetas [34]). The translation stiffness equation is:

$$\frac{K_x(2-\gamma)}{G} = 2.1\left(1+2\frac{B}{D}\right)\left(1+\frac{H}{3B}\right)\left(1+\frac{4H}{3D}\right) \qquad (12)$$

where B is the half width of the foundation, D the depth of the soil layer and H the depth of embedment of the foundation (height of wall).

The rotational stiffness K_θ expressed in dimensionless form is:

$$\frac{K_\theta(1-\gamma)}{G\,B^2} = 1.62\left(1+0.2\frac{B}{D}\right)\left(1+\frac{H}{B}\right)\left(1+\frac{2H}{3D}\right) \qquad (13)$$

Equations (12) and (13) are strictly only applicable for $D/B \geq 2$ and $H/B \leq 2/3$

Figures 33 and 34 show the dimensionless stiffness parameters calculated by Equations (12) and (13) versus the layer depth to wall embedment ratio D/H with the structure half-width to height ratio B/H as a parameter. Also shown on the plots are the stiffnesses calculated by the FEA's carried out in the present analysis for the uniform soil cases. There is reasonable agreement between the analytical and FEA estimates although the FEA result for translation on the deep layer (50 m) is approximately 30% lower than the analytical value. (The curves are truncated at various D/H values because of the limit of applicability of Equations 12 and 13 as indicated above.)

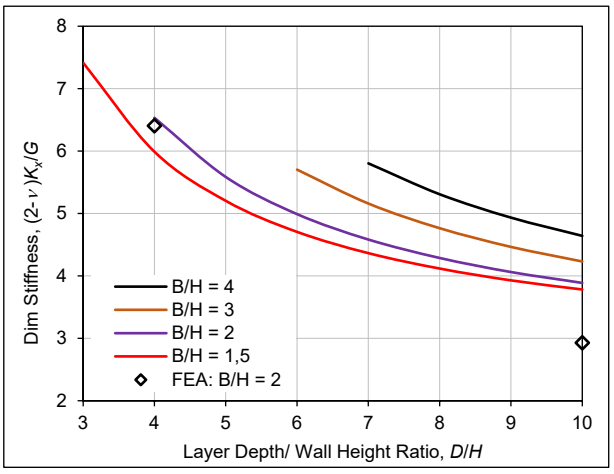

Figure 33: Stiffness of embedded 2-D foundations for translation.

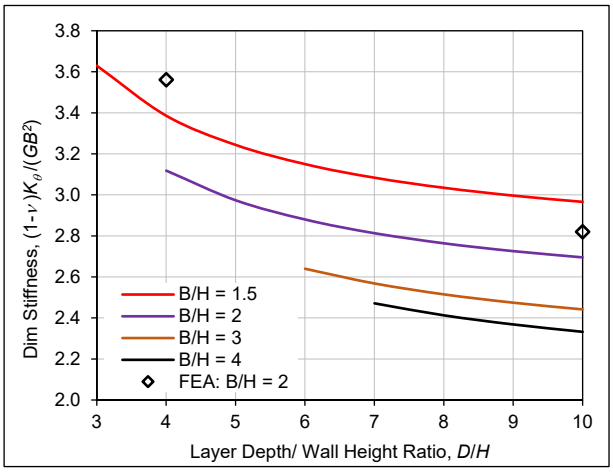

Figure 34: Stiffness of embedded 2-D foundations for rotation.

Figures 33 and 34 show that the layer depth to wall height ratio D/H has a significant influence on the stiffness, particularly for the translation case. The half-width to height ratio B/H also has a significant influence with the stiffness increasing with width as expected. (The reduction in the rotational stiffness with increasing width shown in Figure 34 is because the stiffness has been made dimensionless by dividing by B^2.)

Gazetas and Tassoulas [35] presented horizontal stiffness equations for arbitrarily shaped foundations embedded in a deep layer of uniform elastic soil. Hatzikonstantinou et al [36] presented corresponding stiffness equation for the rocking or rotational stiffness. An advantage of the Gazetas and Tassoulas and Hatzikonstantinou et al stiffness analyses methods is that they apply to any foundation ground plan whereas the Jakub equations given above are only applicable to a foundation plan that has a length much longer than its width. For rectangular buildings located on the ground surface with a half-width of B and a half-length of L, the horizontal stiffness in the width direction, K_{xs} expressed in dimensionless form is given by Gazetas and Tassoulas as:

$$\frac{(2-\nu)K_{xs}}{2LG} = 2 + 2.5\left(\frac{B}{L}\right)^{0.85} \qquad (14)$$

The ratio of the stiffness for an embedded foundation, K_x to the surface foundation is given by:

$$\frac{K_x}{K_{xs}} = \left(1+0.15\left(\frac{H}{B}\right)^{0.5}\right)\left[1+0.69\left\{\left(\frac{H}{L}\right)^2\left(\frac{L}{B}+1\right)\right\}^{0.4}\right] \qquad (15)$$

For rectangular buildings located on the ground surface the rotational stiffness about the longitudinal axis, $K_{\theta s}$ expressed in dimensionless form is given by Hatzikonstantinou et al, as:

$$\frac{(1-\nu)K_{\theta s}}{2LB^2\,G} = 0.62\left(2.4+0.5\frac{B}{L}\right) \qquad (16)$$

The ratio of the stiffness for an embedded foundation, K_θ to the surface foundation is given by:

$$\frac{K_\theta}{K_{\theta s}} = 1 + 1.26\frac{H}{B}\left[1+\left(\frac{H}{B}\right)\left(\frac{B}{L}\right)^{0.5}\right] \qquad (17)$$

Equations (15) and (17) are based on the foundation walls having full contact with the soil. These equations are simplified from more comprehensive equations presented by Gazetas and Tassoulas and Hatzikonstantinou et al that cover the case when the walls are not in contact with the soil over a defined depth below the ground surface.

Figures 35 and 36 show dimensionless translational and rotational stiffness values as a function of the L/B ratio calculated using Equations (15) and (17) with the depth ratio B/H as a parameter. The FEA results from the present study for the 50 m deep uniform stiffness layer (with $B/H = 2$) are shown as isolated points on the figure. The two-dimensional FEA results are only valid for large L/B ratios and therefore have been plotted at a $L/B = 10$. They are in reasonable agreement with the analytical results for this ratio. Results for the FEA of the 20 m deep layer are not shown as this layer was not considered to be sufficiently deep for the analytical results to give satisfactory agreement.

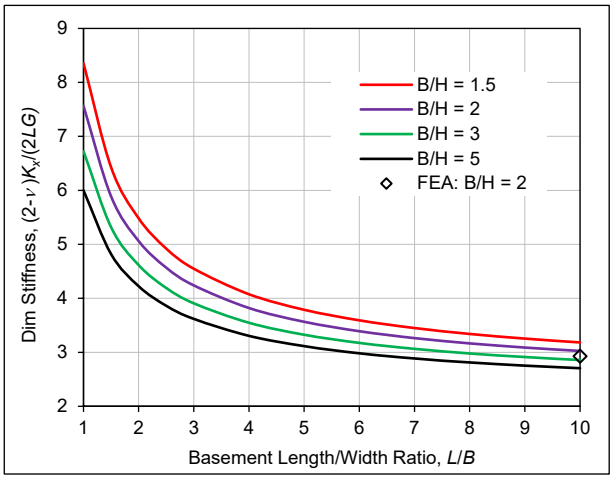

Figure 35: Stiffness of rectangular embedded foundations for translation.

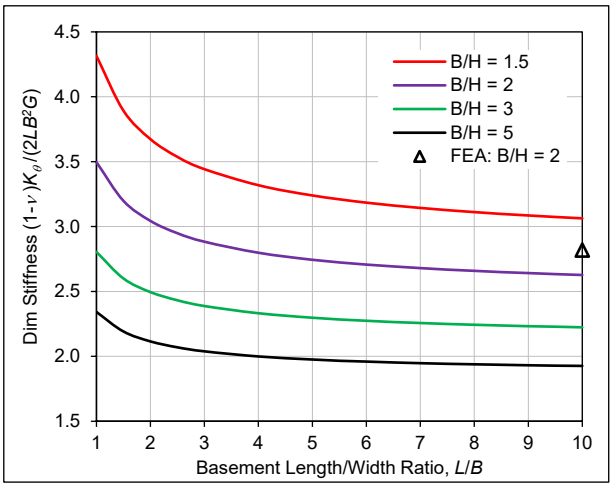

Figure 36: Stiffness of rectangular embedded foundations for rotation.

Figures 35 and 36 show that the L/B ratio has a very significant influence on both the horizontal and rotational stiffness particularly for the horizontal stiffness case. The horizontal stiffness values for $L/B = 1.0$ are at least a factor of two greater than for $L/B = 10$.

The stiffness analytical Equations 12 to 17 are not applicable to buildings that do not have either a long length to width ratio or are not embedded in a deep soil layer. However, the results shown in Figures 33 to 36 can be combined to make preliminary stiffness estimates for buildings that clearly fall outside the bounds of applicability of either the Jakub or the Gazetas and Tassoulas, and Hatzikonstantinou et al sets of stiffness equations.

The analytical stiffness expressions are strictly only applicable to soil layers that have modulus values uniform over their depth. Where there is significant variability with depth using an average value over three times the depth of embedment would be a reasonable approach but further research is required on this aspect.

BUILDING EXAMPLE

In the present study the influence of a building superstructure on the earthquake induced pressures on a basement was investigated by carrying out an analysis of a 7-storey steel framed building located in Christchurch. The main section of the building had a plan area of 17.5 x 51.5 m, a height above ground of 23.8 m, and a total weight including seismic live load of 62.8 MN. The first mode period in the narrow direction, making allowance for the flexibility in the foundation piles, was 0.95 seconds. The building had a basement structure with a depth of 3.3 m and of similar plan dimensions to the superstructure. The basement walls were formed with 250 mm thick precast panels reinforced with HD 12 bars in each face spaced at 200 mm vertically and 300 mm horizontally. The basement was founded on a mix of 1.0 m and 1.2 m diameter reinforced concrete piles. As a simplification for the present analysis, it was assumed that the lateral resistance of the foundation was provided by 24 of the 1.2 m diameter piles which were rigidly framed into the main concrete foundation beams of the transverse superstructure frames. A typical transverse section of the building is shown in Figure 37.

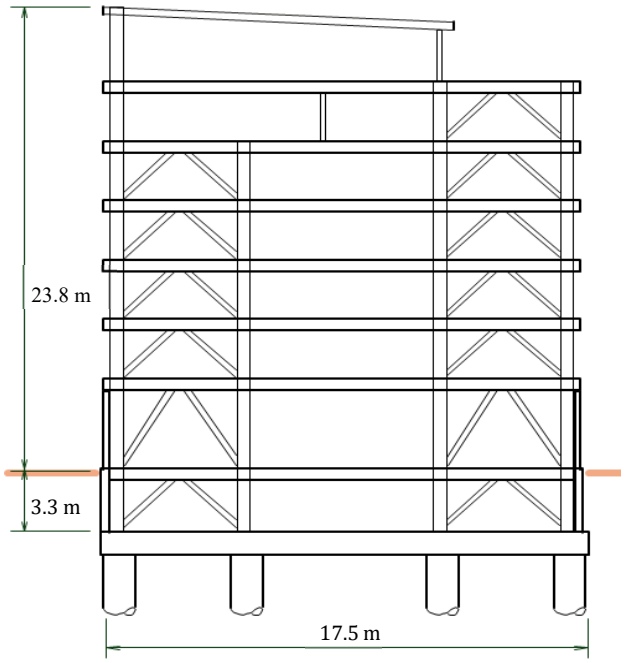

Figure 37: Schematic layout of typical transverse section of 7-storey building.

NZS 1170.5 [9] was used to calculate the design level forces at the interface of the superstructure and basement using a Zone Factor of 0.3, a Return Period Factor of 1.0, assuming Soil Class D and a Ductility Factor of 4. The superstructure base shear and overturning moments were calculated to be 6.8 MN and 108 MN m respectively. An overstrength factor of 2.0 was applied to these actions to calculate the design forces acting on the basement structure.

The site investigation report indicated that the site was underlain with surficial fill and then interbedded moderately loose silts, silty sands and sandy silts to a depth of about 10 m. Below this upper unit there was a thick deposit of fine to medium sands becoming very dense below 12 m. There were interbedded sandy silts, silts and silty sands between a depth of 19 m down to a very dense gravel aquifer at 26 m depth. The

water table was recorded at 1.8 m depth during the investigation. For lateral pile design the site investigation report recommended a Modulus of Subgrade Reaction, n_h of 8 MN/m^3.

The lateral and axial stiffness of the 1.2 m diameter piles was calculated using the elastic continuum method summarised in Pender [32]. The Young's modulus of the soil was assumed to increase linearly from zero at the ground surface with and an increase (m factor) of 8 MPa/m. This increase was consistent with the recommended n_h value and the site SPT N-values that increased in an approximately linear manner from 7 at a depth of 2 m to 90 at a depth of 15 m. For analysis of the basement wall stiffness the Young's modulus at a depth of 3.3 m at the base of the wall was taken as 26 MPa. A Poisson ratio of 0.3 was assumed for the foundation soil surrounding the piles and over the height of the walls. The soil was assumed to have a saturated unit weight of 18 kN/m^3 with the water table below the base of the wall. A bonded contact with the soil was assumed for the walls without any tension gapping.

A lateral stiffness of 3,000 MN/m was calculated for the twenty-four 1.2 m diameter piles assumed fixed by the foundation beams at their heads. From Figure 31 the dimensionless force on the wall was estimated to be 0.26 giving an actual total stiffness of the 51.5 m long wall of 350 MN/m. The lateral deflection of the basement based on the total of the wall and pile stiffness was 4.1 mm giving a force of 1,400 kN on the total length or in dimensionless terms ($P/\gamma H^2$ – where P is force per unit length) a force of 0.15. From Figure 32 the height of the centre of pressure above the base was 0.27 H.

The rotation of the basement under the applied overturning moment was calculated as 0.25 milli radians and is dominated by the axial stiffness of the piles with only a minor contribution in stiffness from the basement walls. From Figure 31 the dimensionless force on the wall assuming rotation about the base was 0.4 ($P/EH\theta$) and a corresponding actual force of 430 kN on the total length. From Figure 32 the height of the centre of pressure above the base was 0.57 H.

Adding the force from translation to the force from rotation gave a total dimensionless force ($P/\gamma H^2$) of 0.19 from the superstructure inertia forces.

Pressure forces on rigid basement walls from soil layer response to the earthquake waves can be estimated using Figure 18. A detailed structural analysis would be necessary to determine the flexibility ratio for the basement structure but the K bracing between columns in the main frames clearly make it a very stiff under horizontal shearing forces. For the present analysis the basement was assumed to be rigid and 17.5 m wide giving a moderately conservative dimensionless force ($P/\gamma H^2$) of 0.8 for a 1 g PGA (this value is reduced by the assumption that the soil modulus is zero at the ground surface and increases linearly with depth over the soil layer). For Site Soil D the PGA for a Return Period Factor of 1.0 is 0.34 g (0.3 x 1.12) giving a dimensionless force from soil layer response of 0.27. The first mode of the soil layer response was estimated to have a period of 0.7 s and because this differed by a moderate degree from the building first mode period it was assumed to be satisfactory to combine the inertia earthquake pressure component (sum of translation and rotation) with the soil layer response component by the SRSS method. This gave a total dimensionless earthquake force on the walls of 0.32. This is higher than the gravity at-rest dimensionless force estimated to be approximately 0.25. An upper bound value of the earthquake force on the wall is obtained by adding the kinematic and inertial components to give a dimensionless force of 0.46. Although clearly conservative the impact of this force might need to be considered for a worst-case scenario. A conservative analysis is required for the pile foundation design and the direct addition of the force on the piles from the sum of the inertial loads from the building response and the pile loads from the kinematic response of the soil layer on the walls should be considered.

For comparison a M-O analysis based on a cohesionless backfill with a friction angle of 32^o gave a horizontal dimensionless total force (including gravity) of 0.28. Subtracting the gravity load component (active pressure) for a flexible wall gave a dimensionless earthquake force component of 0.14. Clearly the M-O assumption of sufficient wall displacement to form an active pressure failure wedge is not satisfied for this basement wall but if the method were used the earthquake pressure force would be grossly underestimated.

Earthquake pressure distributions can be estimated by scaling the pressures shown in Figures 20 for the soil layer response component and Figure 30 (approximate for bonded contact) for the component from the superstructure inertia loads. Figure 38 shows the scaled earthquake pressure components from the superstructure inertia forces acting on the basement and the soil layer response assuming bonded contact for all components. To calculate the total earthquake pressure the translation and rotation inertia components were added and then combined with the soil wave component using the SRSS method. The pressure from an assumed at rest soil gravity load is shown for comparison.

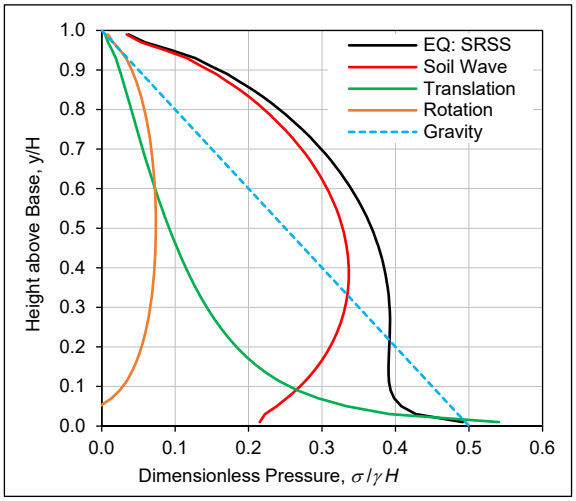

Figure 38: Pressure components on basement wall.

Although load factors commonly applied to gravity only wall pressures may reduce the impact of the gravity and earthquake load combination the calculated earthquake pressures are of sufficient magnitude to need to be considered in the wall design. Gravity and earthquake pressures have different distributions with earthquake pressures higher than gravity in the top section of the wall and this also needs to be considered.

CONCLUSIONS

Currently used analyses methods give a wide variation in the kinematic earthquake induced pressures on basement walls. From the study reported in this paper it was concluded that this issue can be resolved by calculating pressures for design using elastic static or dynamic FEA. Static analyses will give moderately conservative pressures and a refinement is to use the first mode in a simple dynamic modal analysis. This approach was checked by making comparisons with the direct pressure measurements made in centrifuge experiments by Hushmand et al [23] and found to be satisfactory. The method can be extended to include the effects of superstructure inertia forces which may be significant for high-rise buildings.

An elastic FEA basement model with a uniform fine mesh can be set up rapidly in most software packages and will have very

modest compute times on modern laptop computers for both static and modal dynamic analyses. A fine mesh enables the geometry of the basement to be accurately modelled and in most cases a single or several two-dimensional models will be satisfactory. There will be uncertainty in the equivalent elastic properties for the soil but provided the variation with depth is reasonably realistic the results will not be very sensitive to the absolute values of the soil modulus values. An elastic model enables sensitivity analyses to be rapidly carried out using upper and lower bounds for the soil properties to quantify the influence of the soil assumptions on the soil pressures.

There are no simple empirical analytical methods that can adequately cover the wide range of basement and superstructure configurations and the site soil conditions. Nonlinear FEA using time-history acceleration inputs can be used but this adds considerable complexity and may not give more reliable results than a simple elastic FEA. The charts presented in this paper can be used to give an indication of the magnitude of the earthquake induced pressures and whether a more detailed analysis should be carried out.

ACKNOWLEDGEMENTS

Philip Yong of consulting engineers Clendon Burns & Park Ltd consulted the author several years ago on how to estimate earthquake pressures on building basement walls. The author couldn't provide a satisfactory answer or find relevant references for a design procedure so this initiated the work described in this paper. Philip also provided the building example details. My thanks to him for initiating my interest in this topic and providing helpful background material.

The two Reviewers made a number of helpful suggestions that were adopted by the author to improve the paper.

REFERENCES

1 Mononobe N and Matsuo H (1929). "On the determination of earth pressure during earthquakes". *Proceedings of the World Engineering Conference*, **9:** 179-187.

2 Anderson KR, Wood JH and Scott J (2015). "Performance of retaining walls in the Canterbury earthquake sequence". *Proceedings of the 12th Australia New Zealand Conference on Geomechanics.* Wellington, New Zealand. https://www.nzgs.org/libraries/anz-symposium-12-geomechanics-and-human-influence/

3 Dismuke JN (2011). "Retaining wall performance during the February 2011 Christchurch Earthquake". *Australian Earthquake Engineering Society 2011 Conference*, Barossa Valley, Australia. https://aees.org.au/downloads/conference-papers/2011-2/

4 Riches LK (2015). "Observed earthquake damage to Christchurch City Council owned retaining walls and the repair solutions developed". *6th International Conference on Earthquake Geotechnical Engineering*, Christchurch, New Zealand. https://www.issmge.org/publications/online-library?database=59&conference=60&authors%5B%5D=145310

5 Stone EA, Gibson MFL, Wilkins PR and Newby G (2015). "Seismic performance of retaining walls on the Christchurch Port Hills during the 2010/2011 Canterbury Earthquakes". *Proceedings of the 12th Australia New Zealand Conference on Geomechanics.* Wellington, New Zealand. https://www.nzgs.org/libraries/anz-symposium-12-geomechanics-and-human-influence/

6 Wood JH (2014). "Performance of retaining walls in the 2010-2011 Canterbury Earthquakes". *Earth Structures and Retention Conference,* Wellington.

7 Gerstenberger MC, Bora S, Bradley BA, DiCaprio C, Van Dissen RJ, Atkinson GM, Chamberlain C, Christophersen A, Clark KJ and Coffey GL (2022). "*New Zealand National Seismic Hazard Model 2022 Revision: Model, Hazard and Process Overview".* GNS Science Report 2022/57, GNS Science. Lower Hutt, NZ, 106pp. https://doi.org/10.21420/TB83-7X19

8 Stirling MW, McVerry GH and Berryman KR (2002). "A new seismic hazard model of New Zealand". *Bulletin of the Seismological Society of America,* **92:** 1878–1903.

9 Standards New Zealand (2004). *"NZS1170.5: Structural Design Actions. Part 5: Earthquake Actions - New Zealand"*. Standards New Zealand, Wellington, 76pp. https://www.standards.govt.nz/

10 Standards New Zealand (2024). *"Public Consultation Draft, DZ TS 1170.5: Structural Design Actions. Part 5: Earthquake Actions - New Zealand"*. Standards New Zealand, Wellington. 126pp. https://www.standards.govt.nz/

11 Ostadan F (2008). "Seismic soil pressure for building walls– An updated approach". *Bechtel Technology Journal*, **1**(1): 3-12.

12 Schnabel PB, Lysmer JH and Seed B (1972). *"SHAKE: a Computer Program for Earthquake Response Analysis of Horizontally Layered Sites".* Report No. EERC, College of Engineering, University of California Berkeley, California. https://nisee.berkeley.edu/elibrary/getpkg?id=shake91

13 Wood JH (1973). *"Earthquake-Induced Soil Pressures on Structures"*. Report EERL 73-05, Earthquake Engineering Research Laboratory, California Institute of Technology, Pasadena, California. 311pp. https://authors.library.caltech.edu/records/48499-83239

14 Taiebat M, Amirzehni E and Finn WDL (2014). "Seismic design of basement walls: evaluation of the current practice in British Columbia". *Canadian Geotechnical Journal*, **51**(9): 1004-1020. https://doi.org/10.1139/cgj-2013-0212

15 NBCC (2020). *National Building Code of Canada: Volume 1.* Canadian Commission on Building and Fire Codes, National Research Council of Canada. https://nrc.canada.ca/en/certifications-evaluations-standards/codes-canada/codes-canada-publications/national-building-code-canada-2020

16 ASCE (2010). *"Design of Blast-Resistant Buildings in Petrochemical Facilities".* Second Edition, Edited by WL Bounds. 306pp. https://sp360.asce.org/personifyebusiness/Merchandise/Product-Details/productId/232590046

17 Amirzehni E, Taiebat M, Finn WDL and DeVall RH (2015). "Seismic performance of deep basement walls". *6th International Conference on Earthquake Geotechnical Engineering,* Christchurch, New Zealand. 9pp. https://www.issmge.org/events/6th-international-conference-on-earthquake-geotechnical-engineering

18 Mikola RG and Sitar N (2013). *"Seismic Earth Pressures on Retaining Structures in Cohesionless Soils".* Report No. UCB GT 13-01, University of California, Berkley, 217pp. https://nisee.berkeley.edu/elibrary/geotech/2013

19 Candia G and Sitar N (2013). *"Seismic Earth Pressures on Retaining Structures in Cohesive Soils"*. Report No. UCB GT 13-02, University of California, Berkley, 161pp. https://nisee.berkeley.edu/elibrary/geotech/2013

20 Wagner N and Sitar N (2017). "Influence of the depth of embedment on seismic earth pressures on basement walls". *16th World Conference on Earthquake Engineering (16WCEE),* Santiago, Chile, Paper N° 1023, 11pp. https://www.wcee.nicee.org/wcee/article/16WCEE/WCEE2017-1023.pdf

21 Itasca (2012). "*FLAC: Fast Lagrangian Analysis of Continua, Ver. 7.0"*. Itasca Consulting Group Inc., Minneapolis, USA. https://www.itascacg.com/

22 Seed HB and Whitman RV (1970). "Design of earth retaining structures for dynamic loads". *ASCE Specialty Conference, Lateral Stresses in the Ground and Design of Earth Retaining Structures*. Cornell University, Ithaca, New York, 103-147.

23 Hushmand A, Dashti S, Davis C, Hushmand B, Zhang M, Ghayoomi M, McCartney JS, Lee Y and Hu J (2016). "Seismic performance of underground reservoir structures: Insight from centrifuge modeling on the influence of structure stiffness". *ASCE Journal of Geotechnical and Geoenvironmental Engineering,* **142**(7). https://doi.org/10.1061/(ASCE)GT.1943-5606.0001477

24 Brandenberg SJ, Durante MG and Stewart JP (2021). "Single-frequency method for computing seismic earth pressures". *7th International Conference on Recent Advances in Geotechnical Earthquake Engineering and Soil Dynamics*, Singapore: Springer, 1–10. https://link.springer.com/chapter/10.1007/978-981-16-1468-2_1

25 Brandenberg SJ, Durante MG, Mylonakis G and Stewart JP (2020). "Winkler solution for seismic earth pressures exerted on flexible walls by vertically inhomogeneous soil". *Journal of Geotechnical and Geoenvironmental Engineering*, **146**(11): 04020127. https://doi.org/10.1061/(ASCE)GT.1943-5606.0002374

26 Brandenberg SJ, Mylonakis G and Stewart JP (2015). "Kinematic framework for evaluating seismic earth pressures on retaining walls". *Journal of Geotechnical and Geoenvironmental Engineering*, **141**(7): 04015031. https://doi.org/10.1061/(ASCE)GT.1943-5606.0001312#

27 Brandenberg SJ, Mylonakis G and Stewart JP (2017). "Approximate solution for seismic earth pressures on rigid walls retaining inhomogeneous elastic soil". *Soil Dynamics and Earthquake Engineering*, **97:** 468–477. https://doi.org/10.1016/j.soildyn.2017.03.028

28 Durante MG, Brandenberg SJ. Dashti S, Stewart JP and Mylonakis G (2019). "Analysis of seismic earth pressures on flexible underground box structures". *7th International Conference on Earthquake Geotechnical Engineering* – Silvestri, Moraci and Antonielli (Eds), Rome, Italy, ISBN 978-0-367-14328-2 https://www.issmge.org/publications/publication/analysis-of-seismic-earth-pressures-on-flexible-underground-box-structures

29 Durante MG, Stewart JP, Brandenberg SJ and Mylonakis G (2022). "Simplified solution for seismic earth pressures exerted on flexible walls". *Earthquake Spectra,* **38**(3): 1872-1892. https://doi.org/10.1177/87552930221083326

30 NEHRP (2020). "*National Earthquake Hazard Reduction Program: Recommended Seismic Provisions for New Buildings and Other Structures: Volume II: Part 3, Resource Papers, Paper 4, Seismic Lateral Earth Pressures"*. FEMA P-2082. https://www.fema.gov/sites/default/files/2020-10/fema_2020-nehrp-provisions_part-3.pdf

31 Timoshenko S and Godier JN (1951). *Theory of Elasticity.* 2nd Edition. McGraw-Hill, New York. https://www.google.co.nz/books/edition/Theory_of_Elasticity_by_S_Timoshenko_and/ialLYAAACAAJ?hl=en

32 Pender MJ (1993). "Aseismic pile foundation design analysis". *Bulletin of the New Zealand Society for Earthquake Engineering*, **26**(1): 49 – 161. https://doi.org/10.5459/bnzsee.26.1.49-160

33 Jakub M (1977). *"Dynamic Stiffness of Foundations: 2-D vs. 3-D Solutions"*. Publication No R77-36, Department of Civil Engineering, MIT, Massachusetts, 32pp.

34 Gazetas G (1982). "Analysis of machine foundation vibrations: state of the art". *International Conference on Soil Dynamics and Earthquake Engineering*, University of Southampton, England. https://doi.org/10.1016/0261-7277(83)90025-6

35 Gazetas G and Tassoulas JL (1987). "Horizontal stiffness of arbitrarily shaped embedded foundations". *ASCE Journal of Geotechnical Engineering,* **113**(5): 440-457. https://ascelibrary.org/doi/10.1061/%28ASCE%290733-9410%281987%29113%3A5%28440%29

36 Hatzikonstantinou E, Tassoulas JL, Gazetas G, Kotsanopoulos P and Fotopoulou M (1989). "Rocking stiffness of arbitrarily shaped embedded foundations". *ASCE Journal of Geotechnical Engineering*, **115** (4): 457-472. http://dx.doi.org/10.1061/(ASCE)0733-9410(1989)115:4(457)